Universität Zürich[UZH]

An Integrated Vertex Model for Mesoderm Invagination of Drosophila Embryo

Master Thesis

Jianfei Jiang

Physics Institute

University of Zurich

Supervisor: Prof. Christof Aegerter

Contents

Introduction

During the embryonic development of Drosophila, gastrulation is an important step. During this process, cells undergo different paths of development, and the embryo ends up with multiple-layer tissue from a single layer epithelium, which is also seen in other species. Because of its simplicity and tractability, plenty of research has been conducted to investigate the biological basis of gastrulation, especially mesoderm invagination, which is known as an archetypal morphogenetic process showing a collective effect based on individual cell shape change, namely apical constriction. On the biological side, this is a rather complete framework concerning how the mesoderm invagination is promoted, including a detailed genetic control network, cellular force generation, and tissue-wide force propagation. Despite the clarity of its biological background, the role of mechanical forces during the mesoderm invagination and what kind of mechanical properties the tissue should have to promote invagination are not yet clear enough. To answer these questions, people have proposed several physical models that take those ingredients into account, among which vertex models have become a commonly used tool due to their advantages. For example, conceptually, cells are mimicked by a polygon with a certain number of vertices (often a quadrilateral is used in 2D), which makes it easy to assign forces and mechanical properties based on the side and area (or volume). From a practical point of view, simulating a single-layer epithelium does not require high geometrical complexity, which reduces the computational load, and one can still observe realistic behavior from a simple vertex model. In this thesis project, we want to know not only the effects of forces during the invagination but also how the tissue could be affected mechanically. Therefore we present a modified vertex model that treats the cell as an elastic body and has forces assigned to different sides of the cell. First, we studied the forces needed to initiate mesoderm invagination. Then we tried to take the genetic regulation into account to mimic the dynamical forces observed in vivo by setting up reaction-diffusion equations. Finally, we considered a mechanical term based on deformation in these regulating equations acting as a feedback term. The thesis is organized as follows: Chapter 1 describes the biological background of mesoderm invagination from genetic control to mechanical forces. Chapter 2 reviews several fruitful vertex models that manage to give a proper description and prediction. Chapter 3 introduce the methods and results of the thesis project, advantages and defects are discussed in the end.

Chapter 1: Biological Background

In the early development of the Drosophila embryo, epithelial cells will develop through different paths to form three germ layers: the ectoderm, the mesoderm, and the endoderm. This is achieved through a process called gastrulation, during which specific cells will move inward from an outer layer. In Drosophila, this collective cell movement is achieved through the apical constriction that promotes the tissue to form inward curvature, which eventually results in mesoderm and endoderm invagination. The Drosophila embryo is a well-studied system in terms of development, from signals patterning the tissue to cellular structures relative to force generation, and how they are conducted to fold the tissue. For mesoderm invagination (Figure 1), the Dorsal pathway regulates the involved gene expression and eventually leads to a graded distribution of myosin II concentration which creates an apical force gradient and results in apical constriction. In this chapter, the biological background of mesoderm invagination will be introduced, based on both genetic and mechanical aspects starting from the molecular basis.

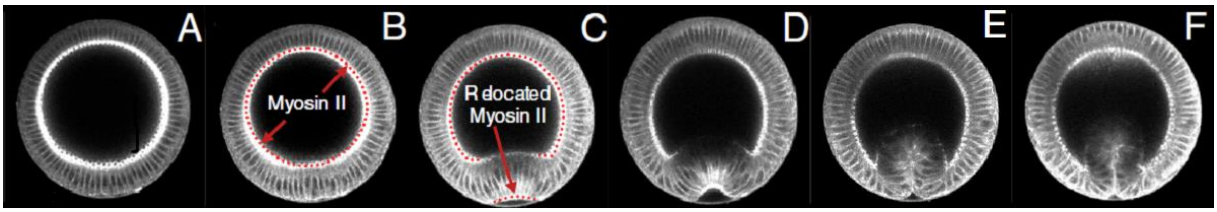

Figure 1 multiphoton images of transverse cross-sections of a wild-type embryo during mesoderm invagination. Embryos are oriented with the dorsal side upward. (Image origin: (Conte, et al., 2010))

1.1 Morphogen gradient

In general, for morphogenesis of the epithelium, morphogens set up a gene expression pattern over the tissue, the resulting signals promote force generation and propagation across the tissue through the cytoskeleton, i.e. actomyosin networks, which causes the tissue to change shape. In Drosophila mesoderm invagination, a morphogen called Spätzle accounts for setting up dorsal-ventral polarity by self-organized shuttling (Haskel-Ittah, et al., 2012). Inactive Spätzle is produced initially and will be activated by cleavage of a protease called Easter within the domain defined by pipe gene expression (Moussian & Roth, 2005). On the lateral side, due to the higher concentration of the Spätzle prodomain, the cleaved Spätzle molecules are more likely to rebind its prodomain to form diffusive complexes. Whereas on the ventral side, more active Spätzle molecules are released and bound with its receptor Toll, which leads to the diffusion of Spätzle-prodomain complexes from the lateral side to the ventral midline (Rahimi, et al., 2019). Diffusion of the complexes establishes a gradient in active Spätzle distribution.

Because Spätzle activates nuclear translocation of Dorsal, Dorsal is also graded with its peak at the ventral midline (Figure 2A). Dorsal has various target genes that control cellular force generation. Those target genes require different activation thresholds (Chopra & Levine, 2009). To promote mesoderm invagination, high Dorsal concentration is needed in order to trigger the expression of *twist* and *snail* acting as positive and negative regulators respectively during the mesoderm invagination (Leptin, 1991). Together with Dorsal, twist and snail can lead to apical contractility and cell shape changes by inducing or suppressing other gene expressions as shown in Figure 2B.

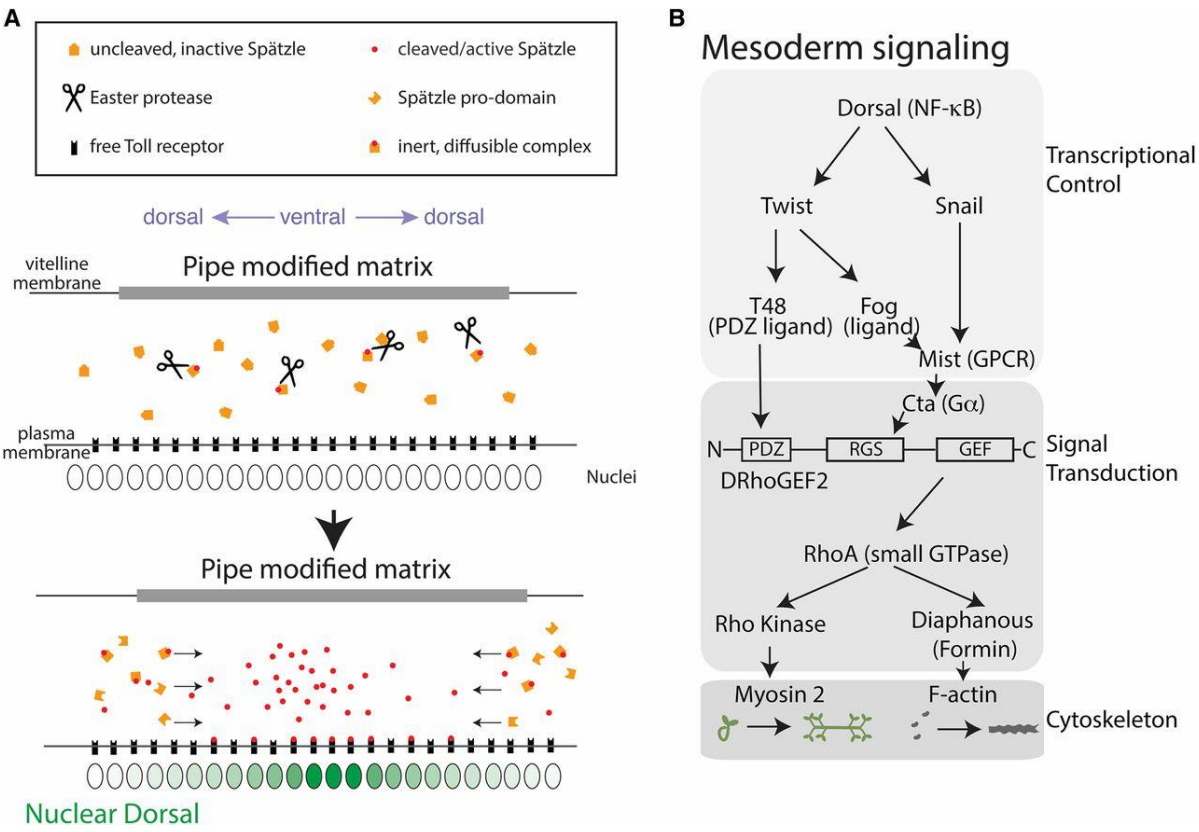

Figure 2 (A) Diagram of Spätzle activation and Dorsal translocation: Easter cleave inactive Spätzle in pipe expression region. Prodomain is preferentially generated outside the pipe region. Cleaved Spätzle binds its prodomain and diffuses toward the ventral midline. Active Spätzle binds Toll receptor leading to Dorsal gradient. (B)Genetic regulation of force generation during mesoderm invagination. (Martin, 2020)

1.2 Functions of twist

Twist functions as an activator that induces the expression of *fog (folded gastrulation)* and a transmembrane protein called T48 to promote mesoderm invagination. Fog is the signaling ligand of a G protein-coupled receptor (GPCR) pathway (Costa, Wilson, & Wiechaus, 1994) that regulates apical contractility. Although mesoderm invagination remains in mutations of the components of this pathway, apical constriction is in an uncoordinated manner: some cells

contract while others are delayed or have abnormal contraction (Martin, 2020). Different GCPR distributions could result in distinct behavior of mesoderm and ectoderm. For instance, A GPCR called Mesoderm-invagination signal transducer (mist) is identified as one of the *fog* receptors which requires *snail* activity (Manning, Peters, Peifer, & Rogers, 2013), whereas another *fog* receptor called Smog appears in the entire embryo (Stephen Kerridge, 2016). Also, discrepancies in GPCR endocytosis between mesoderm and ectoderm contribute to different contractility and determine the extent of the mesoderm (Jha, van Zanten, Philippe, Mayor, & Lecuit, 2018). The fact that ectopic expression of *fog* leads to a rather uniform distribution of apical myosin 2 along dorsal-ventral direction implies *fog* expression should be the main difference between mesodermal and ectopic behavior (Morize, Christiansen, Costa, Parks, & Wieschaus, 1998; Dawes-Hoang, et al., 2005). The mutation of T48 on its own has little effect on mesoderm invagination, however, loss both of T48 and expression of *cta* (a protein-coding gene that accounts for signal transduction in GCPR pathway) leads to a similar result as *twist* mutants, which suggests that T48 and the GCPR pathway regulate mesoderm invagination in parallel (Kölsch, Seher, Fernandez-Ballester, Serrano, & Leptin, 2007). In the sense of myosin II regulations, apical myosin II levels cannot be maintained with disruption of both T48 and *fog*, similarly to mutants with *twist* depletion (Martin, Gelbart, Fernandez-Gonzalez, Kaschube, & Wieschaus, 2010).

There are several other target genes of *twist* that regulate invagination. For example, *snail* expression is mediated by the *twist* in the content of expanding the *snail* domain and maintaining high uniform *snail* levels in the mesoderm (Leptin, 1991). Dorsal and *twist* can intensify the expression of *snail* cooperatively (Ip, Park, Kosman, Yazdanbakhsh, & Levine, 1992). Cell divisions are repressed by the *tribbles* and *frühstart* genes (Grosshans & Wieschaus, 2000; Seher & Leptin, 2000; Grosshans, Müller, & Wieschaus, 2003; Mata, Curado, Ephrussi, & Rorth, 2000), which are regulated by *twist*, otherwise, cell division will disrupt invagination. Another target gene of twist called traf4 is necessary for apical adherens junctions (Mathew, Rembold, & Leptin, 2011).

1.3 Functions of snail

Snail can repress the Bearded family of genes which inhibits the function of the *neutralized* gene (Bardin & Schweisguth, 2006). In mesoderm, the *neutralized* expression is induced by *twist*, it promotes apical contractility through an unknown mechanism (Perez-Mockus, et al., 2017; De Renzis, Yu, Zinzen, & Wieschaus, 2006). This process is suppressed by Bearded proteins in the dorsal ectoderm, but the inhibition cannot happen in the mesoderm due to *snail*

expression that represses the production of Bearded proteins (De Renzis, Yu, Zinzen, & Wieschaus, 2006). In Bearded mutants, the *neutralized* function in ectopic sites leads to increased ectopic contractility that competes with mesoderm invagination, which results in epithelium unfolding even after invagination has started (Chanet & Schweisguth, 2012). Snail also represses *wntD* which is induced by the *twist* in the mesoderm and leads to low expression levels of *wntD*. Furthermore, the *wntD* gene acts as a feedback inhibitor in the Toll/Dorsal pathway, which helps maintain a stable pattern of gene expression downstream of the pathway (Ganguly, Jin, & Ip, 2005). On the other hand, *snail* promotes the expression of *mist* that is mesoderm-specific and required in the GPCR pathway. Mutations in *snail* are unable to activate apical myosin II sufficiently and can no longer exhibit pulsatile apical myosin dynamics (Martin, Kaschube, & Wieschaus, 2009). In comparison to *snail* mutants, *mist* mutants still experience mesoderm invagination (Manning, Peters, Peifer, & Rogers, 2013), suggesting that *mist* is not solely mediated by *snail*.

1.4 Signal transduction

Signal transduction downstream of the GPCR pathway regulated by *twist* and *snail* starts with DRhoGEF2, a guanine nucleotide exchange factor (GEF) for GTPase RhoA (Barrett, Leptin, & Settleman, 1996; Hacker & Perrimon, 1998). DRhoGEF2 responds to upstream production of protein T48 and Gα in a parallel manner. It has an N-terminal PDZ domain to interact with protein T48 that is stimulated by *twist* and acts as PDZ ligand. Another part called regulator of G-protein signaling (RGS) on DRhoGEF2 could interact with the protein Gα expressed by *cta*, which is also induced by *twist.* Additionally, its C-terminal could activate RhoA, and RhoA signaling then results in apical contractility by regulating both myosin II and F actin simultaneously (Kölsch, Seher, Fernandez-Ballester, Serrano, & Leptin, 2007).

Note that RhoA signaling is a dynamic process that leads to ratchet-like contractile pulses of actomyosin activity (Mason, Xie, Vasquez, Tworoger, & Martin, 2016), therefore causing dynamic apical constriction with a series of cell shape constriction and stabilization (Martin, Kaschube, & Wieschaus, 2009). The initiation of contractile pulses of apical myosin II is achieved by activating RhoA signaling through bursts of DRhoGEF2, and the pulse is terminated by a Cumberland G protein activating protein (C-GAP) which represses the RhoA activity (Mason, Xie, Vasquez, Tworoger, & Martin, 2016). Thus a consequence is that, within a period of the pulse, myosin II intensity is increased, then stabilized, cells will undergo a stepwise apical constriction (Martin, Kaschube, & Wieschaus, 2009). Overexpression of C-GAP results in over-depression of RhoA, leading to a relaxation of myosin pulsing to lower

levels than its persistence, accordingly, cell shape relaxation happens instead of ratchet-like contraction (Mason, Xie, Vasquez, Tworoger, & Martin, 2016).

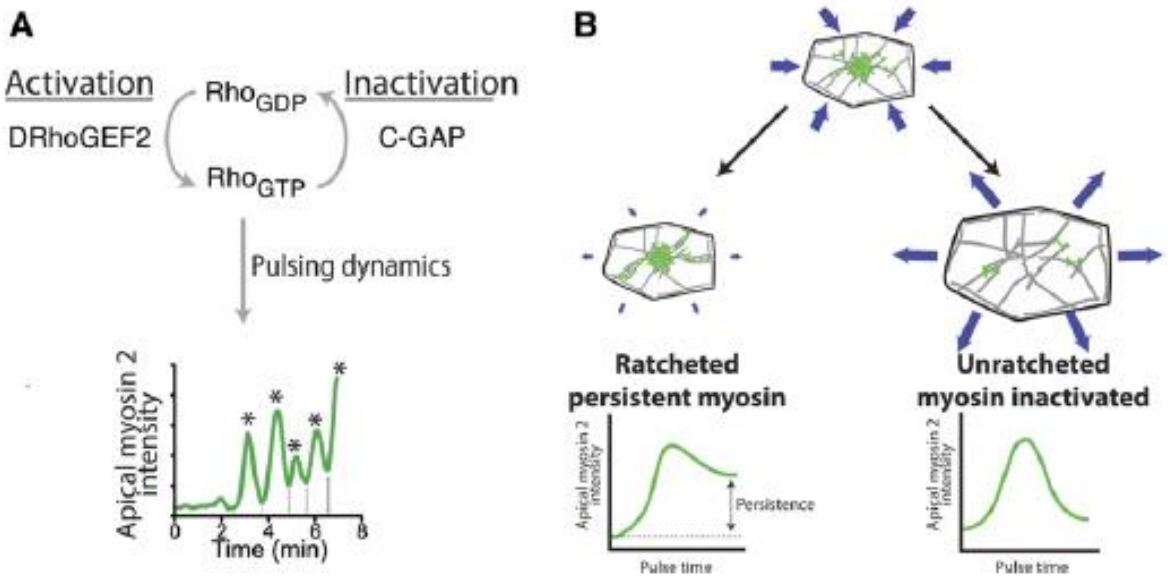

Figure 3 (A)activation-inactivation loop of RhoA leads to pulsatile apical myosin 2 intensity. (B) left: ratcheted constriction with certain persistence; right: overexpression of C-GAP leads to relaxation of myosin 2 intensity. (Martin, 2020)

1.5 Contractile force generation and propagation

RhoA promotes myosin II accumulation through an effector Rho-Kinase (ROCK) that is required in the contracted cells in mesoderm invagination (Dawes-Hoang, et al., 2005). ROCK is required for continuous activation of myosin II, which counterbalances inactivation by myosin phosphatase, otherwise inhibiting ROCK results in the disappearance of myosin 2 (Coravos & Martin, 2016). Note that inactivation by myosin phosphatase is required for the formation of the contractile pulse (Vasquez, Tworoger, & Martin, 2014). Another target of RhoA is F-actin, which is regulated through an effector called formin Diaphanous (Goode & Eck, 2007). Myosin II accumulation happens in the middle of the apical surface where active RhoA and ROCK are located (Mason, Tworoger, & Martin, 2013). F-actin distributes radially with its plus end outward and minus end toward the center forming a contractile unit together with centralized myosin II reminiscent of the sarcomere. This radially polarized arrangement of the actomyosin network results in radially contractile force, generated by myosin II motors, unlike the linear distribution of a sarcomere. (Figure 4B). Importantly, actomyosin networks are dynamic during invagination, spot-like distributions become fibers (Figure 6A) spanning

over the apical surface in response to neighboring mechanical signals, i.e. tissue tension (Chanet, et al., 2017).

In mesoderm invagination, a structure called adherens junction acts as intracellular connection and is responsible to transmit cellular forces across the entire tissue (Dawes-Hoang, et al., 2005; Sawyer, Harris, Slep, Gaul, & Peifer, 2009; Martin, Gelbart, Fernandez-Gonzalez, Kaschube, & Wieschaus, 2010). It contains E-cadherin, an adhesion receptor protein, linking cells on the extracellular side, as well as several adaptor proteins (Figure 4C) on the cytoplasmic side. Thus it connects the receptors to the actomyosin network (Yap, Gomez, & Paron, 2015; Lecuit & Yap, 2015; Vasquez & Martin, 2016). During apical constriction, adherens junctions are pulled centripetally by the contractile force through the actomyosin cytoskeleton (Figure 4A). Depleting components of the adherens junction leads to cell extension, where the cell is pulled toward the cells whose adherens junctions remain (Sawyer, Harris, Slep, Gaul, & Peifer, 2009; Martin, Gelbart, Fernandez-Gonzalez, Kaschube, & Wieschaus, 2010) (Figure 4C).

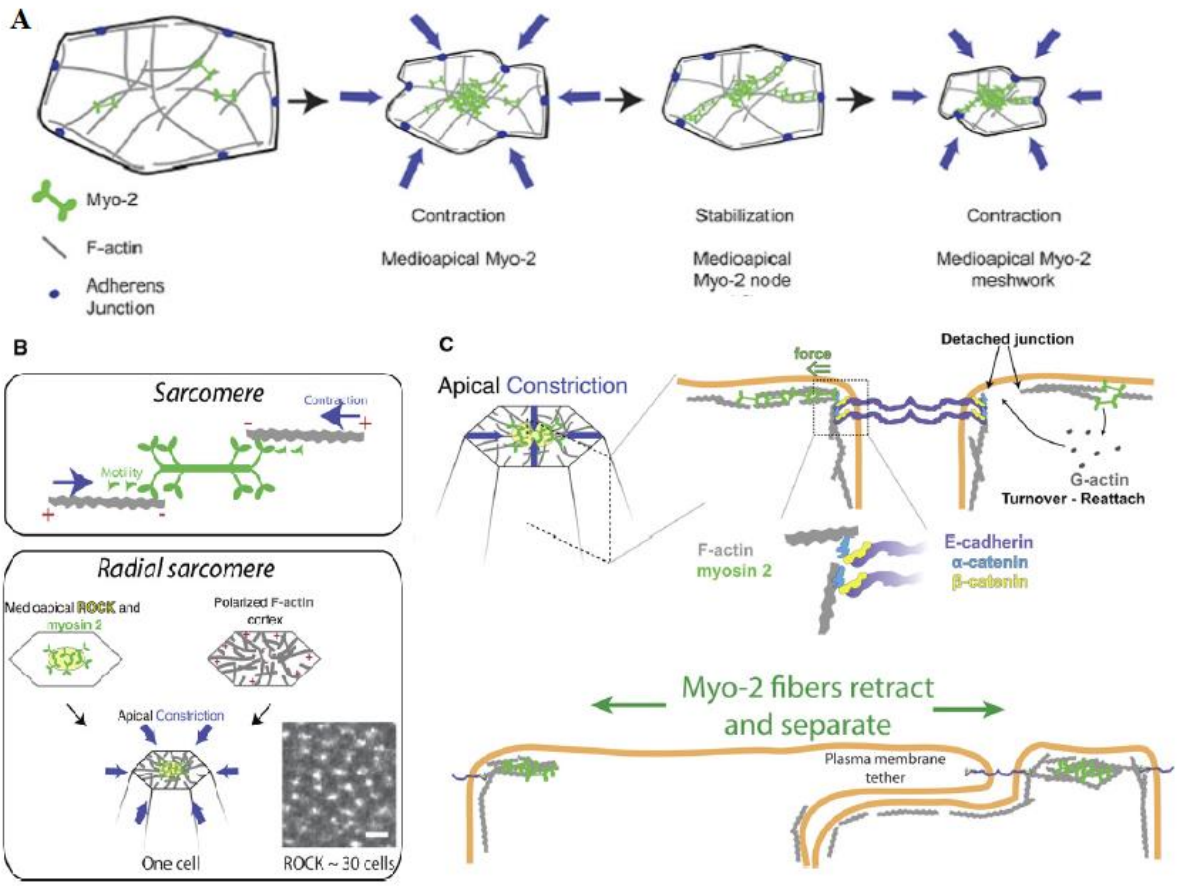

Figure 4 (A) Cartoon shows radial apical constriction by pulling adherens junctions toward the center, and the cell undergoes a series of contraction and stabilization. (B) a contractile unit of sarcomere on the top box, on the bottom box, spatial arrangement of ROCK, myosin II, and F-actin is shown. The image in the bottom box shows a

periodic distribution of ROCK during apical constriction. Bar, 3μm. (C) The cartoon shows the structure and components of the adherens junction on the top, where receptor E-cadherin links cells on the extracellular side and adaptor α-catenin and β-catenin connect actomyosin filaments inside the cell. Detached junction could reattach with help of G-actin; on the bottom, the picture shows a cell with depleted junction components is pulled toward the cell with complete adherens junction. (Martin, 2020)

The transmission of cellular forces to the entire tissue results in global movement and anisotropic tension across the embryo which promotes anisotropic contraction of the apical surface. The highest tension orients along the anterior-posterior axis (Figure 5A), which means that there is greater resistance force to counterbalance the contractile force such that cell shape can hardly change along this direction (Martin, Gelbart, Fernandez-Gonzalez, Kaschube, & Wieschaus, 2010), whereas lower tension along the dorsal-ventral axis leads to cell movement. In addition, a tension gradient is also required in the dorsal-ventral direction during mesoderm invagination (Spahn & Reuter, 2013; Heer, et al., 2017; Lim, Levine, & Yamazaki, 2017). In constricting cells, a graded expression pattern of *twist* is observed (Heer, et al., 2017) (Figure 6B), which results in a myosin II gradient, i.e. a tension gradient. The fact that mutants with ectopic *twist* expression induced by mechanical deformation fail to undergo mesoderm invagination (Farge, 2003) may imply, first, that ectopic *twist* expression flattens the gradient leading to the failure; and second, that cell shape change is a regulatory factor of cell behavior. The anisotropic tension distribution depends on the ellipsoidal shape of the embryo, changing the embryo to a more spherical shape destroys the anisotropy (Chanet, et al., 2017), which also suggests that the tissue shape will feed back on cell movement.

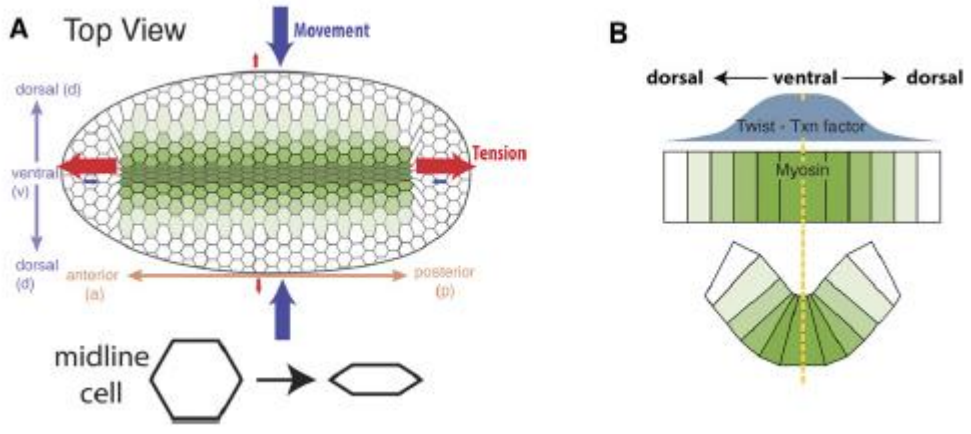

Figure 5 (A) Top view of the embryo, highest tension orients along a-p axis resisting cell shape change while movement happens along the DV axis having lower tension with gradient. (B) Transversal cross-section of constricting cells, graded expression of twist leads to myosin II gradient that provides tension gradients to promote apical contraction. (Martin, 2020)

1.6 mechanical feedback during mesoderm invagination

Another function of the actomyosin cytoskeleton and adherens junctions is to provide mechanical responses through a mechanosensing mechanism (Hannezo & Heisenberg, 2019), in which proteins change their conformation in reaction to the applied force. For instance, in mesoderm invagination, actomyosin fibers align along the anterior-posterior axis where the highest tension orients there. The more they align in the AP direction, the more the cell contracts in the DV direction. Thus the alignment acts as positive feedback that promotes the contraction. In contrast, actomyosin rings are formed in the endoderm where the tissue tension is more isotropic and promotes centripetal constriction (Figure 6A and B) (Chanet, et al., 2017). Mechanical signals contribute to apical myosin II accumulation, but it is not thought to be the primary mechanism (Costa, Wilson, & Wiechaus, 1994; Kölsch, Seher, Fernandez-Ballester, Serrano, & Leptin, 2007; Xie, Mason, & Martin, 2016). Adherens junctions are also not necessary for myosin II accumulation but affect the geometry of actomyosin networks. On the one hand, actomyosin networks remain in fibrous shape in the presence of adherens junctions. With depleted junctions, the spanned actomyosin fibers shrink to spots centralized on the apical surface (Figure 6C). On the other hand, myosin II contractility stabilizes adherens junctions that are disassembled by *snail* in the mesoderm (Weng & Wieschaus, 2016), The fact that repressing ROCK activity results in the decline of E-cadherin shows the dependence between adherens junction stability and myosin II contractility (Figure 6D) (Coravos & Martin, 2016).

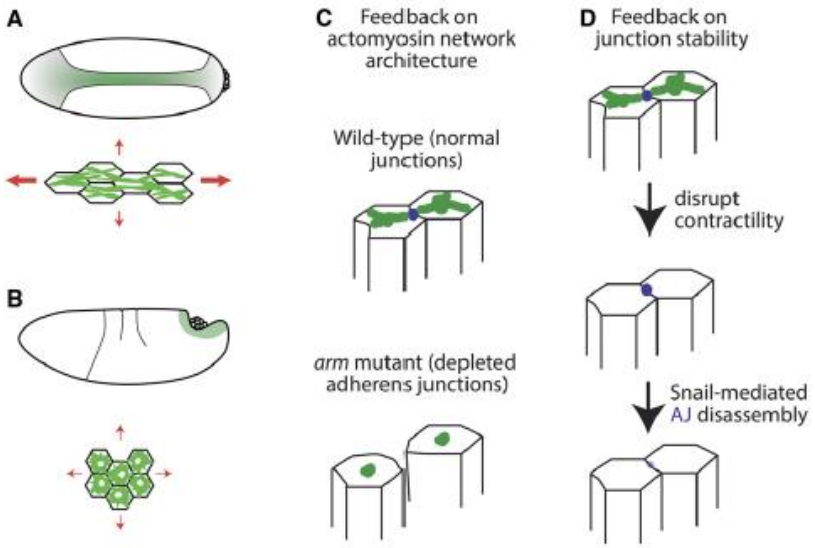

Figure 6 (A) and (B) show the fibrous and ring-like actomyosin in mesoderm and endoderm respectively. (C) shows spot-like actomyosin molecules due to depletion of adherens junctions in arm mutant compared to fiber in wild-type. (D) demonstrates that adherens junctions require myosin II contractility to stabilize in presence of snail-mediated disassembly. (Martin, 2020)

To summarize this chapter, we have talked about the basic biological background of mesoderm invagination. We looked at the genetic control pathway in detail, discussed the initiation of the gradient from morphogen Spätzle to the resulting transcription factors i.e. twist and snail, and downstream to the signals that regulate the cellular force generation. The important point is the regulation resulting in an anisotropic tension across the tissue, such that collective cell shape changes are driven by the graded tension. In addition, mechanical information plays a role in the regulation network, not only in the sense of contributing to myosin II induction but leading to conformational changes of the actomyosin network in reaction to mechanical constraints. With both, autonomous behavior through genetic regulation, and passive response through mechanical feedback, tissue-wide morphogenesis happens in an ordered and robust manner.

Chapter 2: Theoretical Models

To better understand the underlying physical mechanisms of mesoderm invagination, several mathematical models have been developed. A good model should recapitulate cellular behavior in vivo, as well as be able to give predictions that guide experiments to verify if the process is fully understood. Current models can be generally classified into force-based and deformation-based. In 2 dimensions, both share the same framework that cells are simulated by quadrilaterals with 4 vertices for each cell. Cell movements are determined by energy minimization and reflected by the motion of vertices, but the exact energy function differs. It has been shown that considering the 3D cases will not affect the model behavior significantly, therefore, a 2D vertex model is a good approximation for the study of mesoderm invagination. In this section, we will introduce different 2D vertex models and discuss critical mechanisms for invagination, based on the conclusions from those models.

2.1 Excitable (active) viscoelastic model

The pioneering work of modeling epithelial folding is done by Odell et al. (Odell, Oster, Alberch, & Burnside, 1981) in 1981. They assume that the tissue consists of identical cells with predefined viscoelastic properties. The actomyosin filaments on each side are simulated by a viscoelastic unit consisting of a parallelly connected dashpot and spring (Figure 7A).

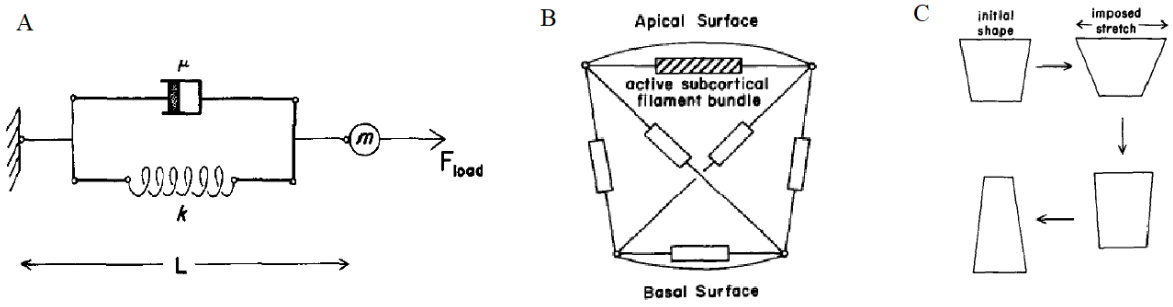

Figure 7 (A) Diagram of a viscoelastic unit to mimic the actomyosin filament, where μ is the viscosity, k is spring constant, m is the mass, F_{load} is the force acting on the filament and L is the length of the filament. (B) The diagram shows the combination of viscoelastic units in (A). (C) sequences of cell shape change once the apical unit is excited. (Odell, Oster, Alberch, & Burnside, 1981)

The motion of this mechanical system is governed by Newton's law:

$$m\frac{d^2L}{dt^2} = -k(L - L_0) + \left(-\mu\frac{dL}{dt}\right) + F_{load} \quad (1)$$

where the first term is the elastic force, the second term is the viscous force, and the last term is the external load exerted by the neighboring mechanical system. Due to the small spatial scale of such a cellular system, the acceleration term is much smaller than the viscous term so can be neglected. Then the equation of motion becomes:

$$\frac{dL}{dt} = -\frac{k}{\mu}(L - L_0) + \frac{1}{\mu} F_{load} \tag{2}$$

To activate the apical constriction, another assumption is put in termed as an excitable system that is specific to the apical surface, where the rest length L_0 varies in time when the spring is stretched. Thus, the unit acts as elastic material for small deformations, while it suddenly reduces its rest length L_0 to reach a stable contracted state if it is stretched larger than a certain threshold. The idea of the stretch-activation mechanism is inspired by smooth muscle cells that undergo a series of contraction, relaxation, and stabilization (Prosser, 1974), like the contractile pulsations (Martin, Kaschube, & Wieschaus, 2009) during mesoderm invagination that was discovered nearly 30 years after Odell's model.

The cell is the combination of the excitable system and viscoelastic components (Figure 7B). The only active excitation unit is assigned to the apical side, diagonal components are used to model the internal viscoelastic properties of the cell, and the cell volume is thought to be constant during the dynamics. Once the apical side is stretched above the threshold, the apical side eventually shrinks due to the reduced rest length, as shown in Figure 7C. The resulting tissue-wide shape change closely resembles the final stage of ventral furrow formation of the Drosophila embryos (Figure 8).

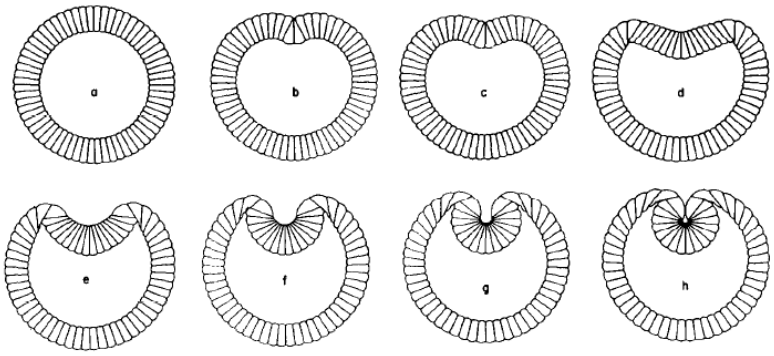

Figure 8 Time series of computer simulation of Drosophila embryo mesoderm invagination (Odell, Oster, Alberch, & Burnside, 1981)

The model suggests that the propagation of contraction waves originating from a single cell is sufficient to promote mesoderm invagination. However the intermediate stages are not observed in vivo, a possible reason may be ignorance of vitelline membrane that is treated as a

boundary condition to maintain a circular shape of the entire tissue in the later model. Although the contraction waves are also not observed in vivo, it was shown that apical constriction is a critical factor of mesoderm invagination. Also, it postulates the presence of the actomyosin network on the apical surface, which had not been described experimentally. This pioneering work provides insights on understanding biological morphogenesis through a purely mechanical approach, rather than digging into the molecular basis.

2.2 Deformation decomposition model

Another approach based on deformation was proposed by Muñoz et al. (Muñoz, Barrett, & Miodownik, 2007) who consider active and passive deformations instead of forces, in addition, the epithelium is treated as a hyper-elastic, non-viscous continuum with prescribed regions of mesoderm and ectoderm, rather than a composition made up of individual cells. The active deformation has two modes: apical constriction and apicobasal cell elongation/shortening. Mesodermal cells are assigned apical constriction and apicobasal elongation modes, whereas ectoderm only has apicobasal shortening during simulations. A vitelline membrane is considered as a rigid boundary and the yolk and cells are assumed to remain constant volume.

The idea of deformation decomposition is to express the total deformation field by multiplication of active and passive parts. The total deformation gradient is given by $\boldsymbol{F} = \frac{\partial \boldsymbol{x}}{\partial \boldsymbol{X}}$, where $\boldsymbol{x}$ is the current position and $\boldsymbol{X}$ is the reference position. An intermediate state $\bar{\boldsymbol{x}}$ is introduced to represent the final shape after applying an active deformation gradient $\boldsymbol{F}_p = \frac{\partial \bar{\boldsymbol{x}}}{\partial \boldsymbol{X}}$, which finally assumes a hyper-elastic deformation from shape $\boldsymbol{x}$ to shape $\bar{\boldsymbol{x}}$, thus giving another deformation field $\boldsymbol{F}_e = \frac{\partial \boldsymbol{x}}{\partial \bar{\boldsymbol{x}}}$, such that $\boldsymbol{F} = \boldsymbol{F}_e \boldsymbol{F}_p$.

The motion is determined by minimizing the strain energy function of a Neo-Hookean hyper-elastic material whose energy density is given by the nonlinear function:

$$\psi = \frac{\mu}{2}(\boldsymbol{F}_e : \boldsymbol{F}_e - 3) - \mu \ln J_e + \frac{\lambda}{2}(\ln J_e)^2 \tag{3}$$

where λ and μ are Lamé's first parameter and shear modulus, both can be obtained from measured Young's modulus and Poisson ratio by relations $\lambda = \frac{\nu E}{(1+\nu)(1-2\nu)}$ and $\mu = \frac{E}{2(1+\nu)}$ respectively, and $\boldsymbol{J}_e = \det \boldsymbol{F}_e$. In the first term, $\boldsymbol{F}_e : \boldsymbol{F}_e$ denotes the first invariant of the deformation tensor.

Different from Odell's model, this model requires experimental measurements as inputs, which allows us to test a set of combinations of active deformations. Regardless of the implementation details of the above equations using e.g. a finite element method, the results show that different contributions of the two active deformation modes affect the final configuration. In Figure 9A, τ_1 represents the contribution of apical constriction and τ_2 corresponds to apicobasal elongation/shortening. α is the ratio between τ_1 and τ_2. It shows that apicobasal elongation promotes the internalization of the mesoderm but fails to form a furrow without enough contribution from apical constriction. With increasing the weight of the apical constriction, a reasonably closed ventral furrow can form, while decreasing the weight of apicobasal elongation reduces the depth of invagination.

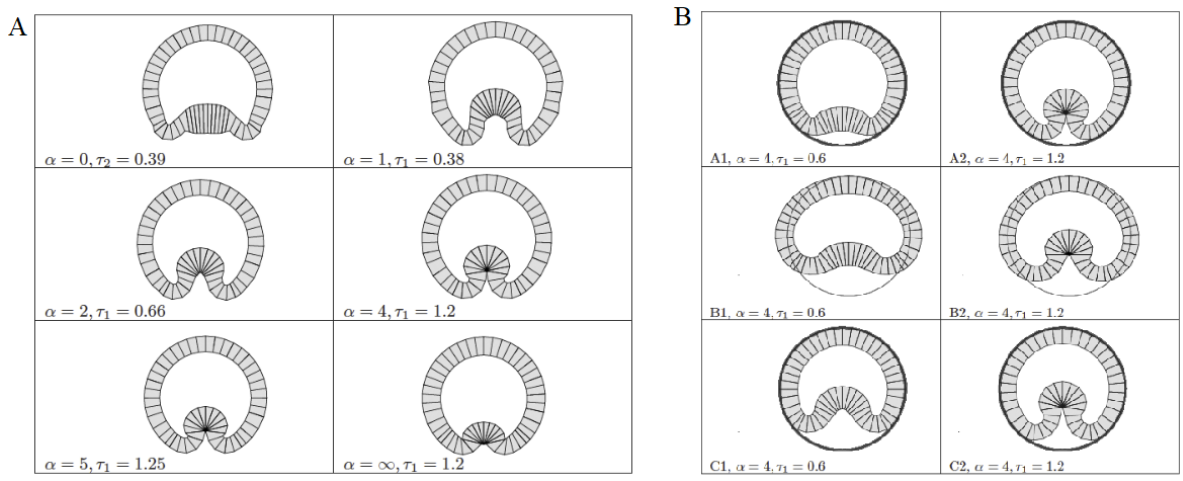

Figure 9 (A) the results of different weights of two active deformation modes, where constant yolk volume and rigid vitelline membrane are applied. (B) part A invagination with vitelline membrane and constant yolk volume, part B only constant yolk volume holds, part C only vitelline membrane is considered. (Muñoz, Barrett, & Miodownik, 2007)

They also studied the role of the vitelline membrane and constant yolk constraint (Figure 9B). The vitelline membrane as a rigid boundary maintains a circular shape of the tissue contributing to closing the furrow. Constant yolk volume should be taken into account in order to get a closed invagination as well.

A more systematical study of this model was done by Conte et al. (Conte, Muñoz, & Miodownik, 2009). A broad range of final shapes is obtained including successfully invaginated and abnormally invaginated i.e. invagination on lateral sides, as well as non-invaginated. They conclude that the decisive deformation that promotes furrow formation is ectoderm shortening because it enlarges the apical length of the ectoderm leading to internalization. However, this

does not agree with experiments. The fact that invagination still happens within embryos whose lateral cells do not behave like ectoderm (Grunewald & Leptin, 1990) may imply shape changes only in the mesoderm are sufficient for furrow formation.

2.3 Collective mechanics

Instead of studying the detailed description for in-vivo invagination behavior, Hočevar Brezavšček et al. (Hočevar Brezavšček, Rauzi, Leptin, & Ziherl, 2012) tried to find out minimal requirements for ventral furrow formation. A more simplified elementary structure is used in their model. The epithelium is modeled by a single layer of identical cells (Figure 10), associated with an energy function containing tensions of the cell cortex (Eq 4). An individual cell is modeled by a quadrilateral: 4 sides and 4 vertices. Line tensions are side-specific and constant cell volume is applied. The energy function of the entire tissue is given by:

$$W = \sum_{i=1}^{N} \left(\Gamma_a L_a^i + \Gamma_b L_b^i + \frac{1}{2} \Gamma_l L_l^i \right) \quad (4)$$

where Γ is the line tension, L is the cell length and i is the cell index, subscripts denote apical, basal, and lateral side correspondingly. The yolk is thought to have constant volume and initial inner pressure p_{int} before buckling of the tissue. The vitelline membrane exerts an extra pressure $p(r) = p_0 \left[\exp\left(\frac{r - r_v}{r_v} \right) - 1 \right]$ onto the part of the tissue outside of a circular boundary with a radius r_v, where r is the distance from the center, and p_0 is set to $10^4 p_{int}$. This extra pressure term provides an energy penalty written as $\sum_{i=1}^{N} p(r) \Delta A_i$ once the tissue moves outside the boundary, where ΔA_i is the area outside the vitelline membrane.

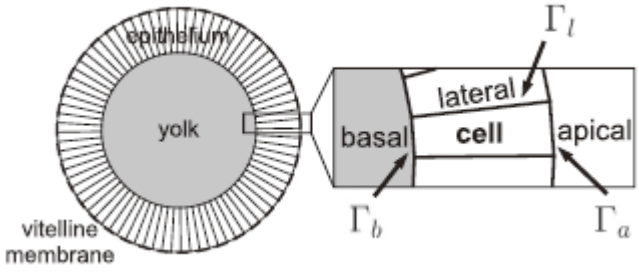

Figure 10 Diagram of the model system (Hočevar Brezavšček, Rauzi, Leptin, & Ziherl, 2012)

The resulting phase diagram of final equilibrium states for relative tensions $\alpha = \frac{\Gamma_a}{\Gamma_l}$ and $\beta = \frac{\Gamma_b}{\Gamma_l}$ exhibits a broad range of invagination patterns (Figure 11). With individually growing α or β (along the vertical or horizontal direction of the phase diagram), or simultaneously increasing α and β (along diagonal $\alpha - \beta = 0$), the depth of internalization decreases, even reaching a

non-invaginated shape for the latter case, which suggests that a relatively large lateral tension is required to form a furrow. Patterns that occur along the diagonal with $\alpha + \beta = const$ are very similar, this could be explained by concerning $\alpha + \beta$ as effective tension acting on the tissue midline (equidistant between apical and basal). If $\alpha + \beta > threshold$, energy minimization results in shrinking or maintaining the length of the midline, which keeps a circular shape. Decreased values of $\alpha + \beta$ lead to the expansion of the tissue midline, as all cells expand collectively the tissue buckles inward due to the additional limit set by the vitelline membrane.

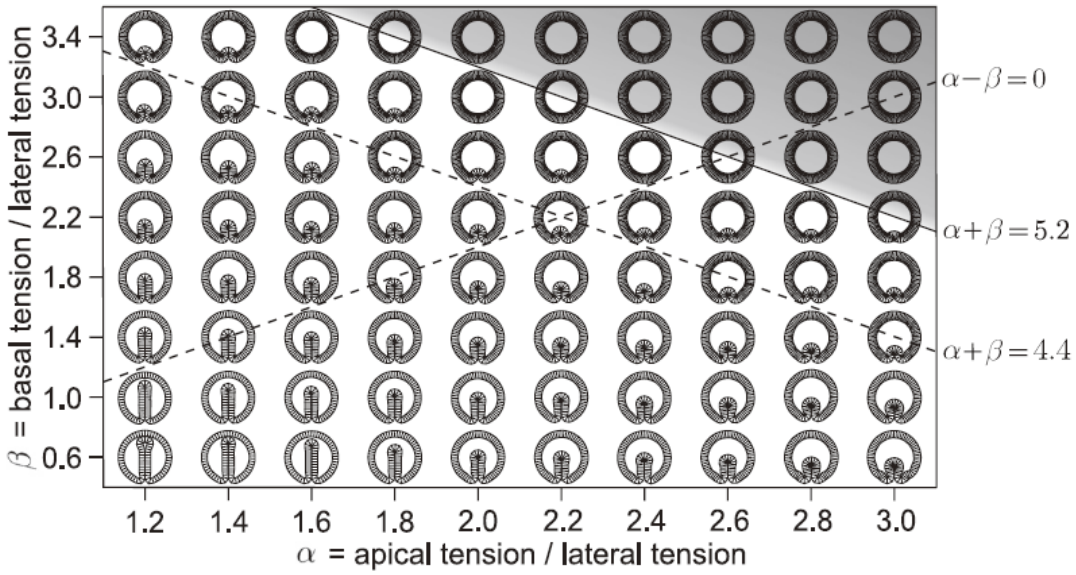

Figure 11 Phase diagram of model embryo cross-section. Non-invagination patterns show up in the shadow area on the top right with small relative lateral tension. Large relative lateral tension leads to deep invagination on the bottom left. (Hočevar Brezavšček, Rauzi, Leptin, & Ziherl, 2012)

Unlike previous models, where mesoderm and ectoderm are manually separated by applying different mechanisms, Hočevar Brezavšček's model uses purely identical cells such that invagination could happen at an arbitrary position whereas in vivo folding always happens in the mesoderm. Thus there should be an asymmetry accounting for the differentiation. Since at the start of invagination mesoderm cells are larger than ectoderm cells by around 30% cross-sectional area. By adding this to the initial configuration, the invagination is controlled to happen within the region having a larger area (Figure 12).

An interesting idea of this model is the hypothesis of collective instability which induces the furrow without any subdivision of the epithelium. This might be an unexplored mechanism and further experiments are needed to validate.

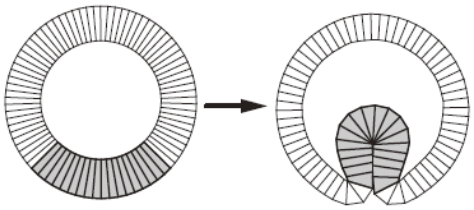

Figure 12 diagram shows that adding asymmetry observed in vivo leads to controlled invagination: the shadowed region has a larger area. (Hočevar Brezavšček, Rauzi, Leptin, & Ziherl, 2012)

2.4 Force-gradient-based model

Cellular force measurements are critical for understanding the underlying mechanics. It is hard to measure the force in all cells during morphogenesis, but video force microscopy (VFM) developed by Brodland et al. (Brodland, et al., 2010) makes it possible to deduce tissue-wide force distributions from live images. The model follows three main steps to obtain the force distribution: first, the epithelium is segmented into polygons with nodes and sides to keep track of them in time; second, an inverse algorithm calculates the net force on each node that can drive the deformation between sequential frames based on a given viscosity; lastly, the algorithm calculates forces along sides that are required for generating the net force. (Figure 13A) The relation between forces and deformations is given by:

$$\boldsymbol{C}_i\left(\frac{1}{\Delta t_i}\boldsymbol{u}_i\right) = \boldsymbol{f}_i \tag{5}$$

where $\boldsymbol{C}_i$ is a finite element-based damping matrix based on given viscosity μ. $\boldsymbol{u}_i$ is the deformation at i-th time step that is retrieved from the images, Δt_i is the time interval, $\boldsymbol{f}_i$ is the computed nodal force. The forces are dynamic during mesoderm invagination: a parabola-shaped time dependence is observed. Also, an apical force gradient is observed, which peaks at the ventral midline and decreases along the dorsal-ventral axis. A recent study (Heer, et al., 2017) shows that the myosin II gradient exists in the mesoderm which confirms the presence of an apical tension gradient from a molecular point of view. Basal tension differs depending on mesoderm or ectoderm. And a radial force (equivalent to later tension) shows a graded distribution on the mesoderm and is constant on the ectoderm. (Figure 13B, C)

In the forward model developed by Conte et al. (Conte, et al., 2012) in 2012, forces from VFM are used as input of numerical simulations where the model tissue is treated in a similar fashion as in VFM. The nodal forces and displacements obey Eq5, but the output now is the displacements. They studied the role of active forces by applying apical, basal, and lateral tension separately at different time points. They concluded that the shortening of the ectoderm

has little effect on furrow formation. This is in contrast to it being a decisive factor in their previous deformation decomposition model (Muñoz, Barrett, & Miodownik, 2007). Apical constriction does not affect the depth of the furrow, but radial tension does.

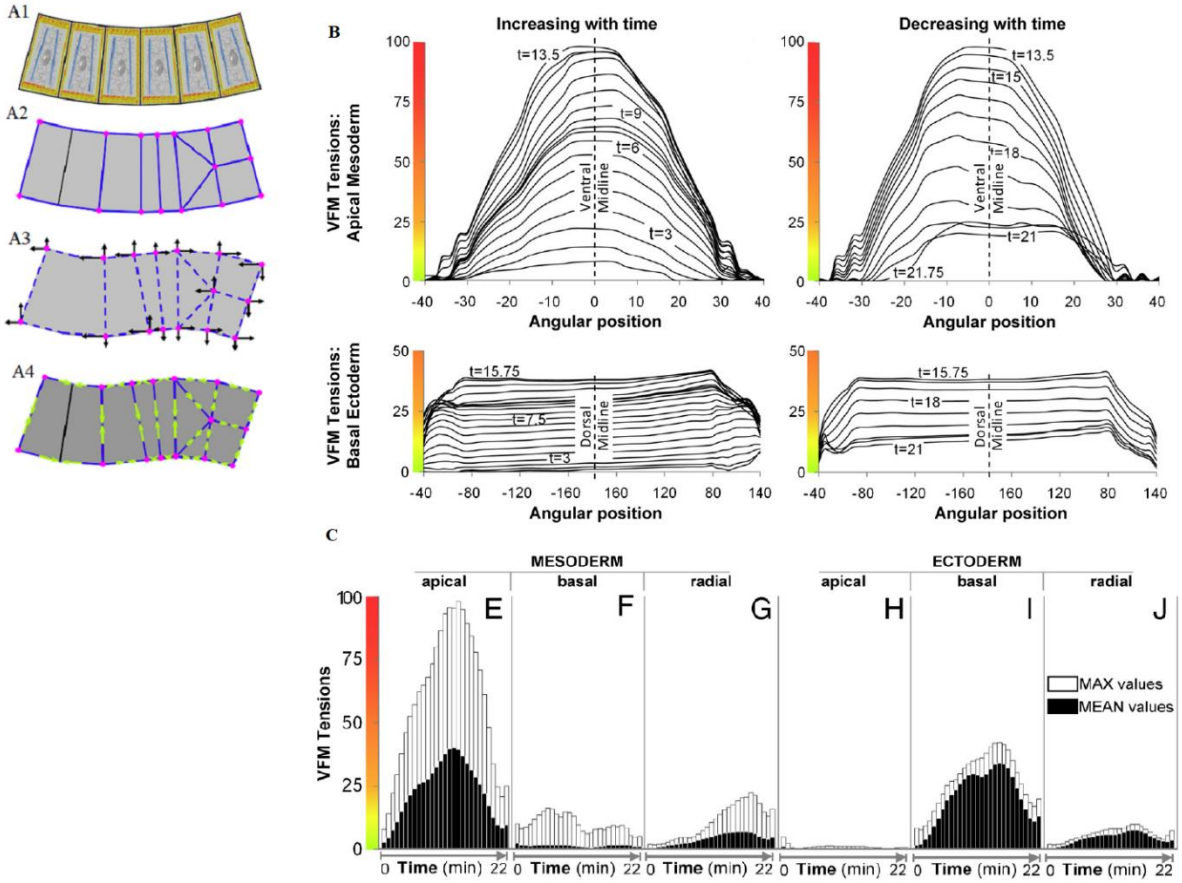

Figure 13 (A) shows the schematic reconstruction steps of edge forces. A1 is the cell image, A2 is the partitioning of the image A1, A3 shows the net forces on nodes (black arrows) and A4 shows the edge forces (green arrows) that are required for the net forces. (B) demonstrates the result of Drosophila mesoderm invagination measured by VFM. (C) shows the time dependence of the active forces, where the white columns are maximal forces and black columns are average forces. (Conte, et al., 2010)

Two years later, in 2014, Polyakov et al. (Polyakov, et al., 2014) proposed a vertex model to explore the effects of passive mechanical response. The surface of each side is considered as an elastic material associated with surface elastic energy (the second term in the square brackets in Eq 6, where a_i, b_i, l_i correspond to the apical, basal, and lateral surface area of i-th cell, index 0 denotes the preferred area. In a 2D cross-section, these areas become side lengths, and volume becomes area). The only active mechanism applied to the model is the apical constriction that is described by a Gaussian function φ_i and a region defining function μ_i (the first term of Eq6). The biological basis of φ_i and μ_i are the gene expression patterns of *twist* and *snail* respectively,

leading to an apical force gradient. Therefore, the overall energy function of the tissue is given by:

$$E = \sum_{i=1}^{N} \varphi_i \mu_i a_i^2 + \sum_{i=1}^{N} [\, K_l (l_i - l_0)^2 + K_b (b_i - b_0)^2 + K_a (a_i - a_0)^2] + \sum_i [C_{VOL}(V_i) + C_{YOLK}(V\_YOLK)] \quad (6)$$

where the last term concerns the constant cell volume and yolk volume constraints. The minimal energy configurations (Figure 14A) show that, first, apical constriction is sufficient to drive a closed invagination with the passive response governed by the tissue's mechanical property; second, a minimal lateral rigidity is required for invagination, otherwise small K_l leads to small inward curvature and thinner mesoderm cell shape; third, in the temporal evolution (Figure 14B), reducing the basal stiffness leads to apicobasal shortening and hence promotes closed furrow formation, which reproduces the basal myosin dynamics observed in vivo (Figure 14C).

We have introduced several theoretical models for mesoderm invagination. Although a collective response of identical cells can lead to tissue folding, apical constriction is thought to be the prior mechanism to promote furrow formation. The method of deformation gradient decomposition focuses on the effect of observed deformations onto the model system by ignoring the required forces, while in other models, prescribed forces are necessary. A force-gradient-based vertex model would be a preferable theoretical framework, because, first, the force gradient is observed experimentally from VFM; second, the fact that graded myosin II generating cellular force is required for invagination, supports the measurement of VFM from a biological perspective.

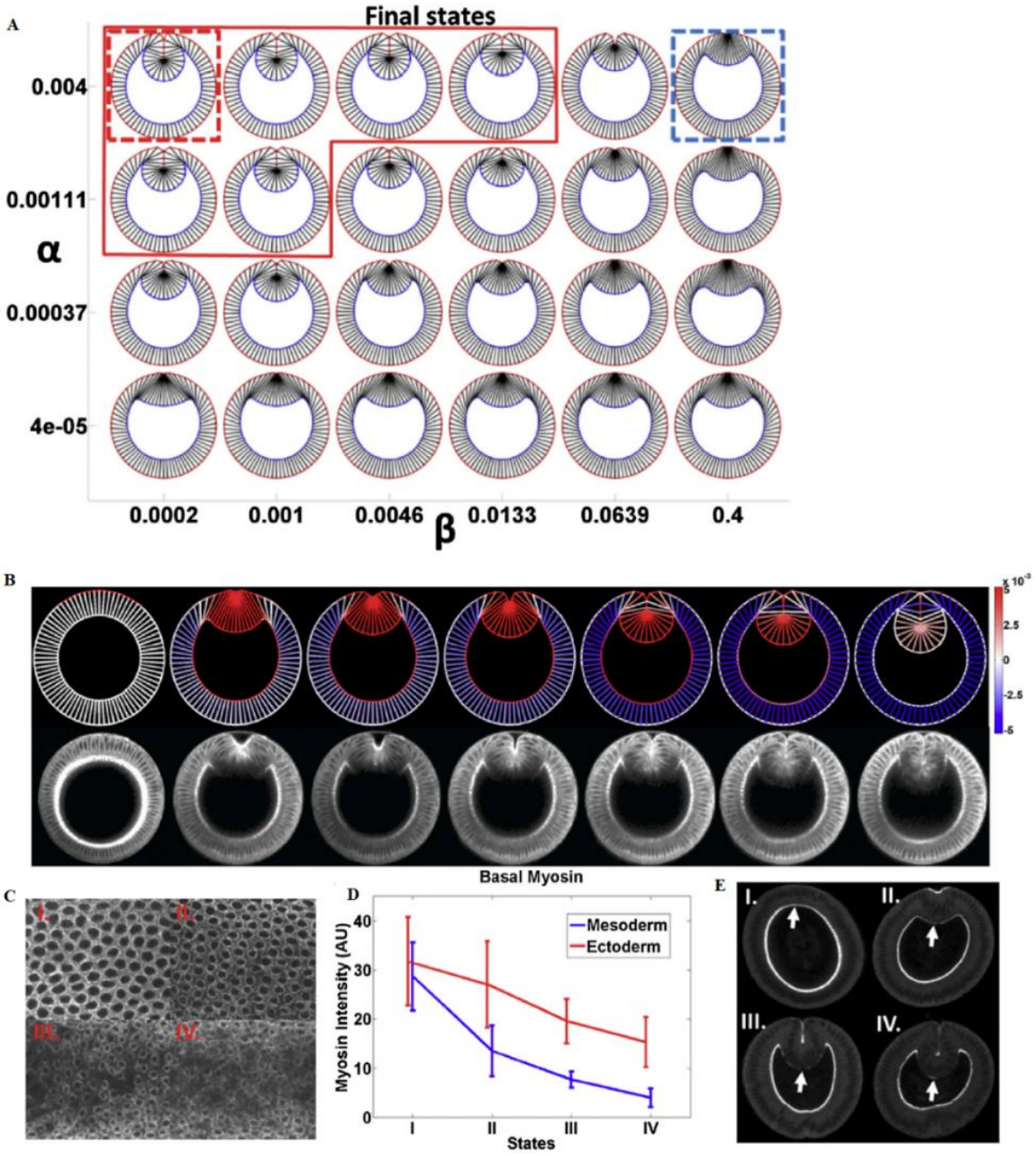

Figure 14 (A) Phase diagram of the final equilibrium shapes. α and β are dimensionless normalized lateral and basal area elasticity constants. Simulations are done with the same apical elasticity. (B) Gradually decreasing basal rigidity closely recapitulates the entire process of invagination. (C) to (E) basal myosin depletion observed in vivo. (Polyakov, et al., 2014)

Chapter 3: Modified Vertex Model

It has been shown that several distinct mechanisms could promote mesoderm invagination in different mathematical models. Our goal is not only to propose modifications of the model but integrate biological regulations and cell movements into a combined model as Aegerter-Wilmsen et al. have done in the growth model of wing imaginal disc (Aegerter-Wilmsen, et al., 2012). To achieve this, we should first have a successful mechanical model governing the cell shape changes, second, we need a concise regulation network that grabs the critical features of the biological process without adding much complexity.

3.1 The mechanical model

The tissue shape change is mediated by using a vertex model assuming cell shape to be quadrilateral as previously described (Hočevar Brezavšček, Rauzi, Leptin, & Ziherl, 2012; Polyakov, et al., 2014). In the 2D case, instead of simulating cell edges with springs that always experience a restoring force, we assume active forces are exerted on each edge; the passive response is achieved by area elasticity. Unlike in the previous model, where constant cell and yolk volumes (2D volume is area) are applied as constraints, we allow them to undergo a small elastic deformation by having a large elastic constant. This approach is similar to Farhadifar's work (Farhadifar, Röper, Aigouy, Eaton, & Jülicher, 2007) modeling the epithelium of Drosophila wing imaginal disc, the difference being that we focus on the transversal cross-section whereas they considered the apical surface and a perimeter elasticity attributed to apical actomyosin rings is included. The potential energy of the tissue is:

$$E(\boldsymbol{r}) = \sum_{i=1}^{N}[\alpha L_a^i(\boldsymbol{r}) + \beta L_b^i(\boldsymbol{r}) + \frac{1}{2}\gamma L_l^i(\boldsymbol{r}) + \frac{1}{2}K_a(A_i(\boldsymbol{r}) - A_0)^2] + \frac{1}{2}K_y\big(A_y(\boldsymbol{r}) - A_{y0}\big)^2 \quad (7)$$

where α, β and γ are the active forces exerted on apical, basal and lateral sides; L_a^i and L_b^i are lengths of apical and basal sides, L_l^i is the sum of two lateral lengths of i-th cell; A_i is the cell area, A_y is yolk area; subscript 0 represents the preferred area; K_x is the area elasticity constant. The vitelline membrane is treated like in Hočevar Brezavšček's model but in a more direct way. The membrane will introduce energetic penalty to potential energy:

$$E_{ext}(r) = E_{press}(\exp(\frac{r-r_0}{r}) - 1) \;\; for\, r > r_0 \quad (8)$$

E_{press} denotes the amplitude of extra energy provided by the membrane, which reflects the radial pressure exerted on the external vertices. This term is set to 0 for vertices inside the

vitelline membrane. r_0 is the radius of the membrane, which is set to the initial radius of the apical surface.

3.2 Implementation details

To implement the vertex model, we use an apical force gradient to promote mesoderm invagination. Thus, the apical line tension coefficient α is spatially dependent, i.e. we choose a Gaussian distributed apical tension:

$$\alpha(n) = \alpha_0 \exp(-\mu(n - n_0)^2) + \alpha_1 \tag{9}$$

μ defines the mesoderm size, n_0 is the cell index of ventral midline and n is the cell index, α_0 is the amplitude and α_1 represents overall apical tension level.

The net force exerted on each vertex is obtained from the negative gradient of potential energy in Eq 7. A straightforward way is to calculate the energy gradient numerically by using the finite difference method, Eq 10, for the x component, and an analog for the y component. Choosing Δx as small as possible increases the precision, while also increasing the computational cost.

$$F_{x_i} = -\frac{\partial E}{\partial x_i} \cong -\frac{E(x_i+\Delta x)-E(x_i)}{\Delta x} \tag{10}$$

The energy gradient can also be computed analytically, giving an expression of force on cell i:

$$\boldsymbol{F}_i = -\sum_{l\in \mathrm{N}_i}\left[\alpha\nabla_i L_a + \beta\nabla_i L_b + \frac{1}{2}\gamma\nabla_i L_l + K_a(A_i - A_0)\nabla_i A_i(\boldsymbol{r})\right] + K_y\left(A_y - A_{y0}\right)\nabla_i A_y(\boldsymbol{r}) \tag{11}$$

For area gradient, any polygon area can be expressed as

$$A = \frac{1}{2}\left|\sum_{i=0}^{n-1}(x_i y_{i+1} - x_{i+1}y_i)\right| \tag{12}$$

where n is the number of nodes of the polygon. Thus the area gradient is given by:

$$\nabla_i A = \frac{1}{2}\begin{pmatrix} y_{i+1}-y_{i-1} \\ x_{i-1}-x_{i+1} \end{pmatrix} \tag{13}$$

For length gradient, the length between two neighboring vertices is:

$$L = \sqrt{\left(x_i - x_j\right)^2 + \left(y_i - y_j\right)^2} \tag{14}$$

Then the gradient is:

$$\nabla_i L = \frac{1}{L}\begin{pmatrix} x_i - x_j \\ y_i - y_j \end{pmatrix} \tag{15}$$

By applying the expressions of Eq 13 and 15 carefully to Eq 11, one can get the force analytically. It is easy to verify that both approaches of getting the force are equivalent. But there are several practical differences. For instance, the numerical method is more direct but less precise and less computationally efficient. Because the model system contains 80 cells, 160 vertices, which is not an enormous computational load, in this case, numerical gradient calculation is convenient to implement and debug without losing much performance.

If the net force on each vertex is known, the motion of the vertex is thought to be overdamped (Darsdo, 2000; Fletcher, Osborne, Maini, & Gavaghan, 2013) with its inertial terms neglected since they are small compared to the dissipative terms, which leads to an equation of motion for the vertex:

$$\eta_i \frac{d\boldsymbol{r}_i}{dt} = \boldsymbol{F}_i \tag{16}$$

η_i is the drag factor of vertex i. Discretization of Eq 16 gives the update rule of vertex position.

$$\boldsymbol{r}_i(t + \Delta t) = \boldsymbol{r}_i(t) + \frac{\Delta t}{\eta}\boldsymbol{F}_i \tag{17}$$

Note that the energy gradient and Eq 17 are solved simultaneously for all vertices in order to avoid any bias from updating sequentially. The implementation steps of the vertex model can be summarized as follow:

1. Update cells properties: lengths, area, tensions, etc.
2. Loop over all vertices to calculate force by Eq 10.
3. Update positions based on Eq 17 for all vertices in parallel.
4. Update stops after a given amount of time.

Whether or not the final equilibrium shape is found depends on the time interval and the number of time steps. The smaller the time interval is chosen, the smoother the motion will be, and the more time steps are required to reach the final equilibrium. To balance the computation time and the quality of the final shape, we set the number of iterations to be a large enough and fixed number, therefore after >50,000 iterations, the model will be at least around the equilibrium. Practically speaking, it is not necessary to use a while loop with a fine precision threshold to find an exact equilibrium state, because we use a fixed step gradient descent method which

always leads to oscillations around the equilibrium, and states near the equilibrium have final shapes that are similar to what we expect for the equilibrium state.

With the current model setup, we can have mesoderm invagination as shown in Figure 15. The problem is that cell overlap happens among invaginated cells shown in Figure 15A. This can be resolved by adding an energetic penalty for vertices inside the tissue, but a simpler way is to add adhesion energy (Eq 18) to vertices that are symmetric about the ventral midline (Figure 15B).

$$E_{ad} = \begin{cases} Ad. & if\ \ d < d_0 \\ 0 & else \end{cases} \tag{18}$$

d is the distance between vertices, d_0 is the reference distance, adhesion occurs only within that distance, Ad is constant adhesion energy. The exact expression of adhesion is not important, the point is that the adhesion term makes invaginated cells stick to each other rather than overlap. Cell and Tissue-specific coefficients are shown in Table 1, and they are consistently used in all subsequent simulations.

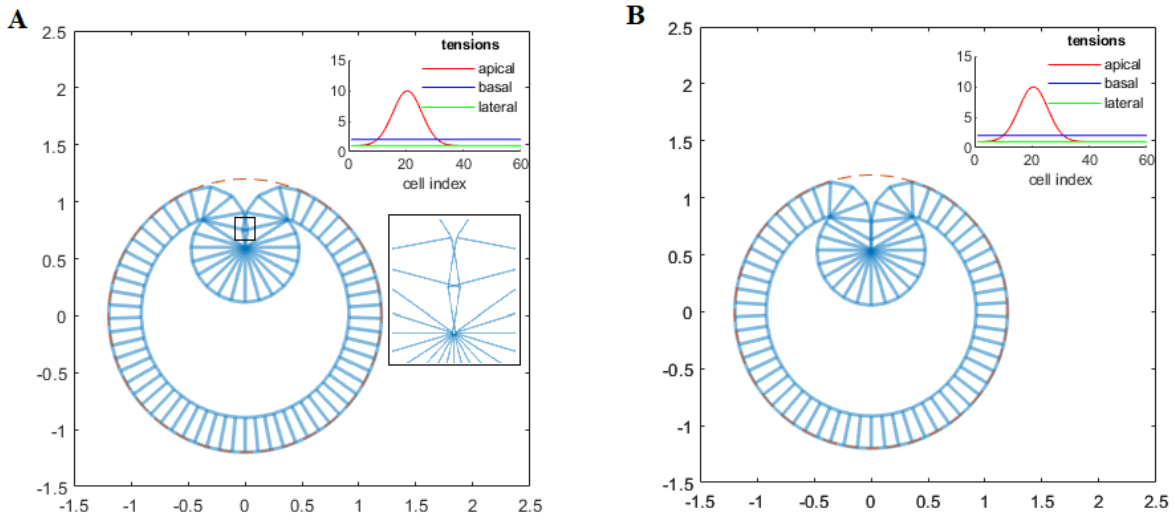

Figure 15 (A) no adhesion term, overlapping occurs in the invaginated cells as shown in the black box. 6×10^4 *iterations in total. (B) adhesion term resolves overlapping.* 10^5 *iterations in total. Inset shows the active tension profile, where* $\alpha_0 = 9, \alpha_1 = 1, \beta = 2, \gamma = 1$.

Table 1 Tissue-specific constants used for simulation

K_a	K_y	A_0	A_{y0}	r_0	E_{press}	μ	η	dt	Ad	d_0
10^4	10^2	0.0314	2.0086	1.2	10	0.02	1	1.5×10^{-4}	10	0.0471

Another problem that could occur during the implementation is basal vertices may move into the tissue at both sides of the basal constriction center (data not shown). This failure results from large lateral forces compared to apical and basal forces. In general, this model artifact should be removed by a repulsive energy term as in the previous model (Polyakov, et al., 2014). However, based on the relative magnitude of active forces observed by VFM (Conte, et al., 2010), the lateral tension should be small compared with the other two. Thus, keeping lateral tension small prevents the model from failing. Hence, it is unnecessary for additional consideration if we can keep parameters in the proper domain, which also avoids increasing model complexity. Also, note that parameters used in the simulation are pure numbers, the real units are not essential because the real values should scale with those parameters. The critical part is the relations between those parameters.

3.3 Results of static tension

The current setup enables us to study the effects of static active tensions on mesoderm invagination. As described above, lateral tension is expected to be smaller compared with the other two active tensions. We first want to know what will happen if lateral tension is larger within the parameter domain where the model works properly. According to the VFM results, the average lateral tension level is around 1/10 of maximum apical tension (Figure 13B), thus a reasonably high ratio of lateral and apical tension could be 2.5/10. We vary α_0 and α_1 to maintain the maximum apical force being 10, meanwhile, we change β to obtain a series of final shapes that reflects the effect of global apical tension and basal tension in response to higher lateral tension (Figure 16).

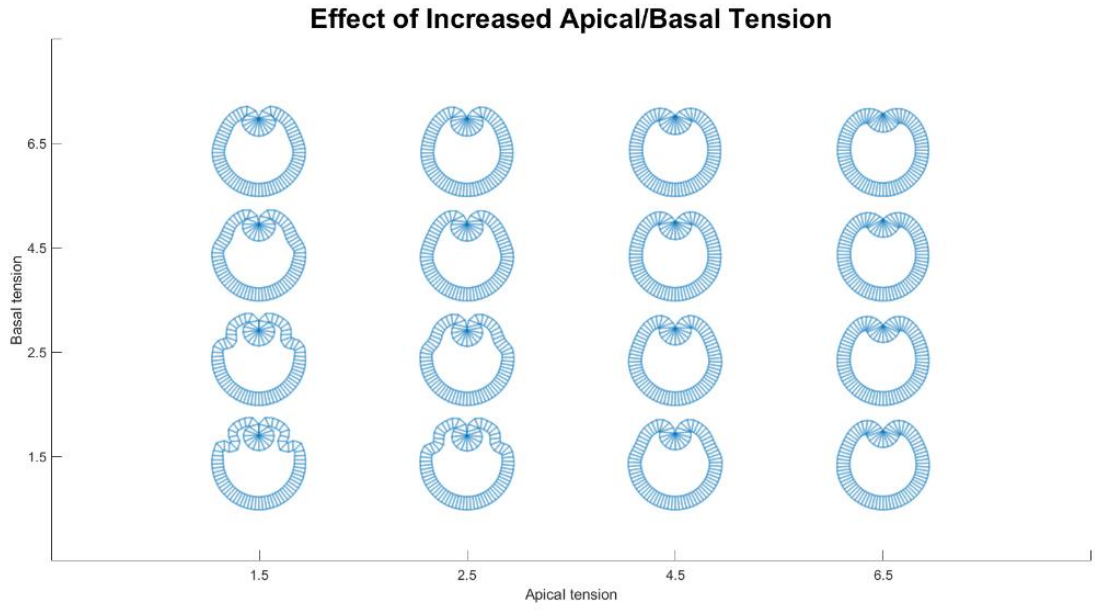

Figure 16 A phase diagram about the increased overall level of apical force (α_1) and basal (β) when lateral tension is high ($\gamma = 2.5$). $\alpha_0 + \alpha_1 = 10$ is kept. 50,000 iterations for the final states.

Abnormal deformations occur at both lateral sides of the mesoderm when α_1 and β are small. This might be explained as disruption of force balance on involved vertices. Apical constriction leads to nonequilibrium of the tissue. Due to large lateral tension, apical vertices are pulled inward. To sustain the cell area with the least elastic energy, basal vertices are pushed inside, which is possible since we allow the yolk to undergo elastic deformation, and the yolk elastic constant is set to be smaller than the cell's, meaning that the yolk is more likely to deform. The energetic benefits of the abnormal deformation compensate for the elastic energy of compressing the yolk. The vitelline membrane limits the deformations happening only within the circle. Therefore, large lateral tension will not pull the basal vertices outward. Increasing either the global apical tension α_1 or the basal tension β prevents the tissue from the abnormal shapes, results in a circular outline, but also prevents it from apicobasal shortening since lateral tension is weak relative to global apical tension or basal tension, suggesting that lateral tension should be at a level that is large enough to promote apicobasal shortening and small enough to maintain a circular shape. To summarize, overall apical tension α_1 and basal tension β help sustain a circular contour on the apical and basal side respectively while lateral tension contributes to apicobasal shortening.

The next step is to find out the effect of lateral and basal forces with a given apical force. We fix α_1 to be 1 and α_0 to be 9, such that the maximum apical tension is still 10. From the discussion above, lateral tension should be small, thus we let it vary in the range between 0.5 to 1.5. And basal tension ranges between 1.5 to 5.5. We obtain another phase diagram shown in Figure 17.

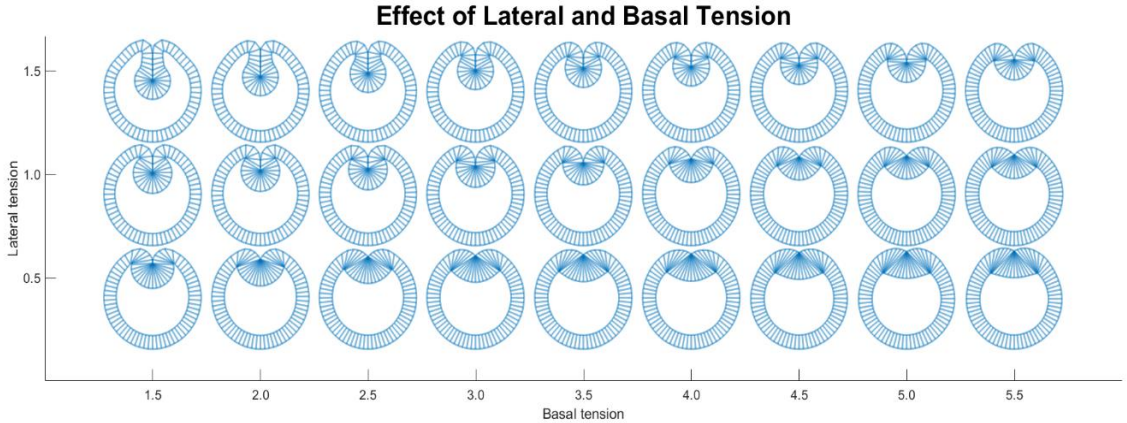

Figure 17 Phase diagram of fixed apical tension.

Along the horizontal axis, raising basal tension flattens the inward curvature, whereas, along the vertical axis, the furrow depth is getting larger with increasing lateral tension. Our model exhibits similar behavior to Conte's model (Conte, et al., 2012), in which apical constriction plays little role in the determination of furrow depth, the critical effect is the promotion of the curvature, and internalization depth is governed by radial shortening force, namely lateral tension. The final shapes correspond to different stages of mesoderm invagination. On the bottom right of Figure 17, the tissue undergoes apical constriction as well as apicobasal elongation. On the top left, tubular furrow formation happens. That may explain the time evolution of the tissue shape. The invagination process might be described as follows: first, an apical tension gradient is set up and promotes apical constriction in the mesoderm, where apicobasal elongation also happens associated with the contraction due to a passive cellular response; later, basal tension drops and lateral tension grows, which cooperatively leads to internalization. Decreased basal tension results in a circular-shaped furrow, the strength of lateral tension determines furrow depth. In contrast to Polyakov's model, our model implies that active basal and lateral forces can also facilitate ventral furrow formation.

3.4 Results of dynamic tensions

Active tensions are probably dynamic during mesoderm invagination (Conte, et al., 2010). Regardless of the mechanism governing the dynamics, we examined our model using tensions with prescribed time dependence.

VFM result (Figure 13) suggests parabolic time dependence of tensions. Instead of using the exact measurements, we generate the dynamic tensions by a parabolic function:

$$f(t) = -\frac{f_{max}}{t_m^2}(t - t_m)^2 + f_{max} \tag{19}$$

in which $f(t)$ is the force at time t, f_{max} is the desired maximum value of the force, t_m is the time point when $f(t)$ reaches f_{max}. Eq 19 determines the lateral tension and the maximum value of apical tension. For simplicity, we assume that there is no spatial dependence on lateral and basal tension. The decrease of the basal tension is described by a sigmoid function:

$$f(t) = \frac{A}{\exp(\kappa(t - t_0)) + 1} + B \tag{20}$$

A is the height, B is the minimal stationary value, κ determines the rate of decrease from maximum to minimum, t_0 is the time when the half-maximum amplitude is reached. Table 2 shows parameters used for Eqs 19 and 20, where N is the total number of iterations.

Table 2 coefficients for prescribed tension dynamics

$f_{max_{apical}}$	$t_{m_{apical}}$	$f_{lateral}$	$t_{m_{lateral}}$	A	B	κ	t_0	N
10	$0.5N$	1	$0.7N$	3	2	$20/N$	$0.5N$	10^5

Since basal myosin II intensity is at a higher level at the onset of gastrulation, we set the initial value of basal tension at 5 and let it deplete regulated by Eq 20. The time dependence with parameters given in Table 2 is shown in Figure 18. We tried several different cases to verify that basal tension depletion and lateral tension increase are both essential for furrow formation.

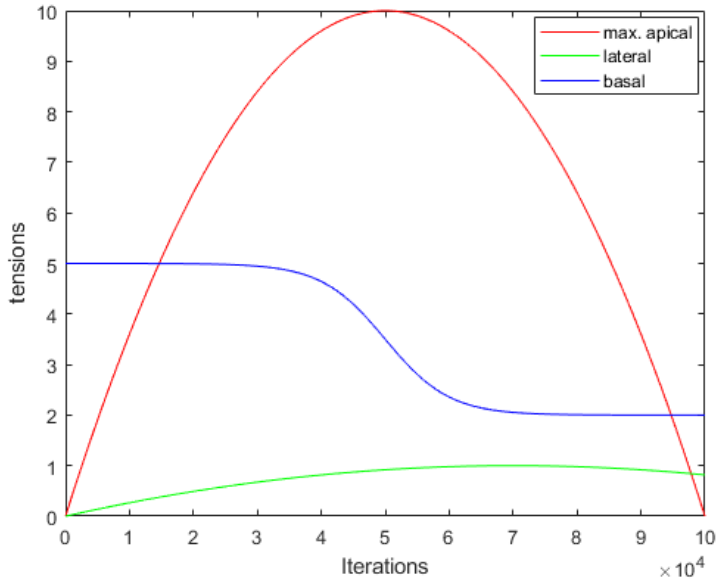

Figure 18 prescribed time-dependence of tensions

First, we examined whether only apical constriction can lead to a fully invaginated shape. We only apply dynamic apical tension whose maximum value is shown in the red curve in Figure 18. The resulting shapes (Figure 19) at different times demonstrate that apical contraction cannot promote a tubular furrow alone, the only effect is to activate internalized curvature, which is consistent with the conclusions from static tension. Because of 0 lateral tension, mesoderm cells undergo apicobasal elongation which makes them thinner, we cannot observe apicobasal shortening in this case.

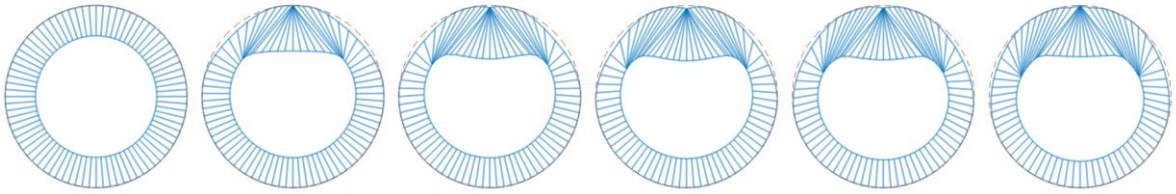

Figure 19 Shapes of different stages during simulations and are in time-order. Only apical constriction is applied. 0 lateral tension and initial basal tension is set to 5 without depleting. The time interval between successive frames is 20% of the total simulation time. Other parameters are the same as Table 1 and Table 2.

Then we added basal force depletion and lateral force increment separately to apical contraction. It turns out that neither can lead to fully invaginated furrow unless all three mechanisms are involved. Lack of basal force depletion results in insufficient internalization (Figure 20A) while lack of increasing lateral force leads to failure in activating apicobasal shortening (Figure 20B). With both mechanisms, a tubular and closed furrow has formed (Figure 20C).

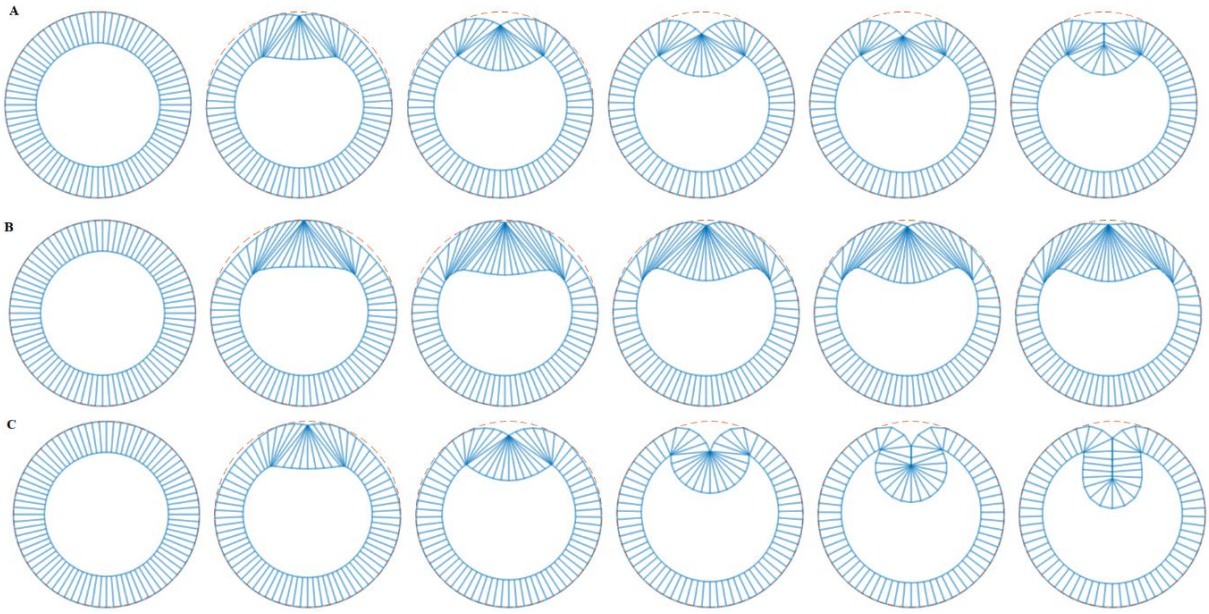

Figure 20 (A) Apical constriction & increasing lateral force (B) Apical constriction & decreasing basal force (C) Apical constriction, basal force depletion & lateral force increasing. The time interval between successive stages is 20% of the total simulation time. Other parameters are the same as Table 1 and Table 2

So far, we could conclude that the absence of either one of lateral force increase and basal force decrease, or both, fails to prompt mesoderm invagination. In other words, radial shortening force is required as in Conte's model (Conte, et al., 2012). A recent study has confirmed the necessity of apical-basal force, mesoderm invagination does not proceed if such a force is disrupted (Gracia, et al., 2019). Decreasing basal force may be attributed to basal myosin II depletion observed by myosin staining (Polyakov, et al., 2014).

3.5 Integrating Regulation equations and cell movement

In this part, we will introduce regulation equations governing the tension dynamics. Since the entire genetic pathway is complicated, a feasible way to describe regulatory behavior is to skip intermediate factors. The gene *twist* acts as an activator that establishes apical myosin activity. We make use of the Gierer-Meinhardt equation (Gierer & Meinhardt, 1972)for *twist* as an activator:

$$\frac{dC_{twi}}{dt} = \frac{p_{twi}C_{twi}^2}{1+K_{twi}C_{twi}^2} - u_{twi}C_{twi} + p_0 \exp(-\mu(n-n_0)^2) \tag{21}$$

Eq 21 describes the dynamics of *twist* production, in which C_{twi} denotes the concentration. Myosin activity is directly related to *twist* concentration. We assume that apical and lateral myosin intensities, as well as depleted basal myosin, are positively correlated with C_{twi}. We construct the remaining equations as follow:

$$\frac{dC_{Amyo}}{dt} = p_A C_{twi}^2 - u_{myo}C_{Amyo} \tag{22}$$

$$\frac{dC_{Bmyo}}{dt} = -lC_{twi}^2 + p_B C_{Bmyo} - u_B C_{Bmyo}^2 \tag{23}$$

$$\frac{dC_{Lmyo}}{dt} = p_L C_{twi}^2 - u_{myo}C_{Lmyo} + p_{L0} \tag{24}$$

In the above equations, p denotes production rate of corresponding substances specified by its subscript, u_{myo} is the myosin breakdown rate, C_i is the concentration of substance i. Eq 22 and 24 share a similar structure since assumed a positive correlation between lateral/apical myosin intensity and *twist* concentration, a slight difference is that Eq 24 contains a constant production term p_{L0} which is expected to account for lateral force increment. Eq 23 describes the time evolution of basal myosin. The first term indicates basal myosin loss due to *twist* expression; the second part is logistic growth governing the global basal myosin depletion. Translating concentration to tension is achieved by multiplying a factor f which could vary based on different tension. With parameters given in Table 3, we could generate the dynamic tensions shown in Figure 21.

Table 3 parameters of regulation equations

p_{twi}	u_{twi}	p_0	K_{twi}	μ	p_A	u_{myo}	l	p_B	u_B	p_L	p_{L0}	f
1	0.8	1.5	1	0.02	0.75	1	0.03	0. 25	0.1	0.15	1	1

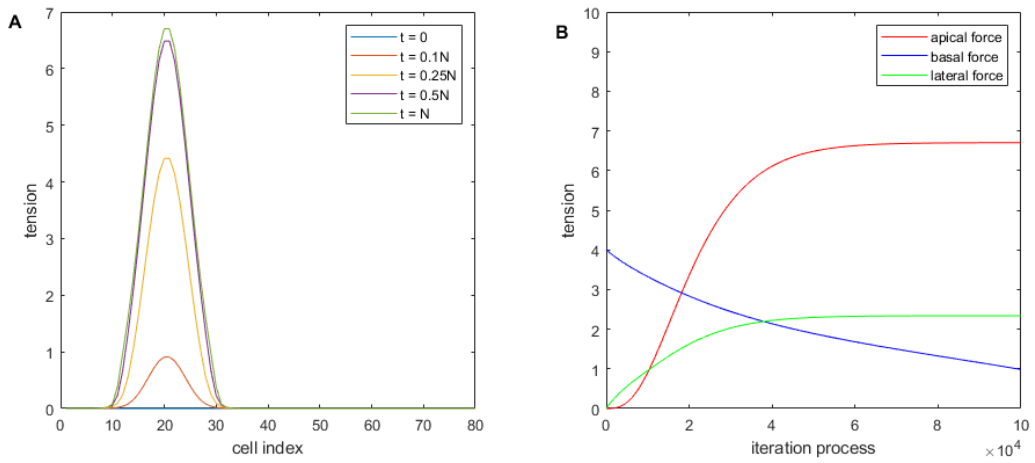

Figure 21 (A) spatial dependence of apical tension at different times (B) time dependence of forces at the ventral midline

Our equations manage to reproduce apical myosin gradient, basal depletion, and lateral increment. In addition, mechanical information could induce *twist* production as shown by Farge's experiment (Farge, 2003). To take such mechanical effects into account, we modify the last term of Eq 21 as follows.

$$\frac{dC_{twi}}{dt} = \frac{p_{twi}C_{twi}^2}{1+K_{twi}C_{twi}^2} - u_{twi}C_{twi} + p_0\frac{P^q}{P^q+H^q} \tag{25}$$

$$P = a\exp(-\mu(n-n_0)^2) + b\frac{\Delta L^l}{\Delta L^l+H_m^l} \tag{26}$$

Total production term P in Eq 25 is given by Eq 26, where a Gaussian term governs genetic control, and a Hill function governs mechanical response. ΔL is the deformation of apical length from its rest value. a and b specify the relative contribution of each term. H and H_m are values when the corresponding Hill function reaches its half-saturation value. The exponents q and l describe the steepness of transition. Both terms share the same saturation value of *twist* production described by the Hill function in Eq 25 to avoid extremely high production at the ventral side where both genetic and mechanical terms are highest. Also, this management equally treats mechanical and genetic terms as input of the overall production. The bias is only determined by the contribution factors a and b.

For implementation, discretizing Eq 25, 22, 23, 24 yields the following updating rules:

$$C_{twi}(i,j+1) = C_{twi}(i,j) + \left(\frac{p_{twi}C_{twi}^2(i,j)}{1+K_{twi}C_{twi}^2(i,j)} - u_{twi}C_{twi}(i,j) + p_0\frac{P^q}{P^q+H^q}\right)\times\Delta t \tag{27}$$

$$C_{Amyo}(i,j+1) = C_{Amyo}(i,j) + (p_AC_{twi}^2(i,j) - u_{myo}C_{Amyo}(i,j))\times\Delta t \tag{28}$$

$$C_{Bmyo}(i,j+1) = C_{Bmyo}(i,j) + (-lC_{twi}^2(i,j) + p_B C_{Bmyo}(i,j) - u_B C_{Bmyo}^2(i,j)) \times \Delta t \quad (29)$$

$$C_{Lmyo}(i,j+1) = C_{Lmyo}(i,j+1) + (p_L C_{twi}^2(i,j) - u_{myo} C_{Lmyo}(i,j) + p_{L0}) \times \Delta t \quad (30)$$

Together with Eq 10 and 17, we obtain updating rules for the integrated model. In the above equations, *i* denotes the current cell index, *j* current time step. During each iteration, do the following computation:

1. Calculate energy gradient for all vertices (Eq 10) and perform the movements (Eq 17).
2. Calculate apical lengths of updated vertices for mechanical feedback
3. Update concentration of all substances (Eq 27-30) and translate them into tensions.

3.6 Results of the integrated model

During the simulations, tissue-specific constants are shown in Table 1, and regulation coefficients are from Table 3. In Eq 26, we assumed equal contributions from genetic and mechanical terms by setting a and b to 0.5. Hill coefficients, l, and q, in Eq 26 and 27 are set to 8 and 3 respectively. The transition points H and H_m are 0.3 and 0.1. Note that the large Hill coefficient in Eq 26 enables a rapidly switching behavior for the mechanical term so that mechanical information acts as a trigger. The small Hill coefficient in Eq 27 allows a smoother transition from low production levels to saturation. We examined several configurations.

First, our integrated model can reproduce the normal invagination process (Figure 22).

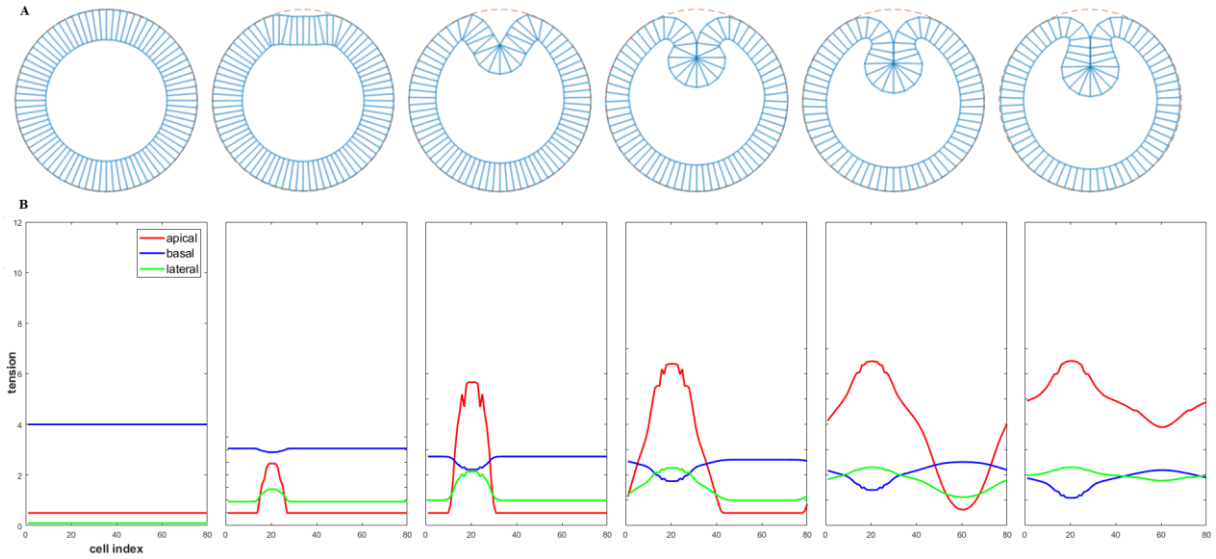

Figure 22 (A) normal invagination process in time sequence. Tensions are governed by regulation equations. The time interval between successive frames is 20% of the total simulation time. (B) corresponding tension profiles of (A). The red line is apical tension, the blue line is basal tension, and the green line is lateral tension.

Although the intermediate shapes do not strictly replicate the deformation observed in vivo, it ends up with a closed furrow. The deviation from the observed deformation may result from early activation of lateral tension increase (Figure 22B). The mesoderm directly bends inward, rather than undergoing apicobasal elongation and shortening in series. The abnormal apical contractions in the mesoderm might be attributed to the mechanical feedback term in Eq 25. That term positively feeds back onto the *twist* production in the compressed cell of the mesoderm, and negatively in stretched cells of the ectoderm. Thus, in our model, the apical tension in the ectoderm is raised to maintain the apical lengths around the rest lengths. The flattened apical force gradient does not prevent invagination from proceeding, which suggests that after internalized curvature has formed, lateral tension plays a more critical role in furrow formation. Despite the differences between simulations and in-vivo observations, our model can successfully invaginate in a robust manner in presence of mechanical feedback.

To investigate the influences of the mechanical term in Eq 27, we tried to mimic the situation that the tissue is under different mechanical constraints. For example, according to Farge's experiment (Farge, 2003), ectopic compression leads to ectopic *twist* production and stops the invagination process. Experimentally, pressing the coverslip on the embryo leads to elliptic compression. To implement the elliptic compression in our simulations, a straightforward way is to set the vitelline membrane to be an ellipse. We applied 20% compression in the direction transversal to the DV axis and 20% extension along the DV axis. We performed energy minimization to find the initial equilibrium for the new boundary. Then the simulation started from that elliptic initial shape.

Compressed tissue does not proceed with mesoderm invagination anymore, although there are anomalous apical constrictions along with the tissue. (Figure 23) The anomalies are symmetrically distributed along the circumference of the embryo. This is because, at those spots, cells are compressed apically, and those compressions exceed the threshold and trigger the positive feedback onto *twist* production, leading to apical constriction. Around the end of the DV axis, either on the ventral or dorsal side, the cells are apically stretched, and the mechanical term acts as negative feedback to keep the apical lengths within a certain tolerance. Even though mesoderm cells still have higher tensions, the gradient has been flattened by the mechanically induced *twist* production, such that mesoderm invagination stops. The mechanical term and the Gaussian term are treated in parallel and share a common saturation value as indicated by Eq 26 and 27, which makes the gradient flattening possible. Otherwise, the positive feedback would lead to a high production rate in the mesoderm and the *twist* gradient would remain. In

addition, the tension profiles are abnormally oscillatory, which may result from the mechanical term, where the Hill coefficient is set to 8. The even number of Hill coefficient makes Hill term in Eq 26 sensitive to the absolute value of deformation. Either compression or extension can induce *twist* productions. That is also why the mechanical term behaves differently in the compressed and stretched cells. In spite of the abnormal contractions, mesoderm invagination does not proceed when elliptic compression is applied. Our model also replicates the ectopic *twist* production, which smears out the *twist* gradient, thus resulting in a flatter apical force profile. The incompleteness of our regulation equations might be the reason for those anomalies. There should be other mechanisms and regulatory rules to avoid unexpected deformation.

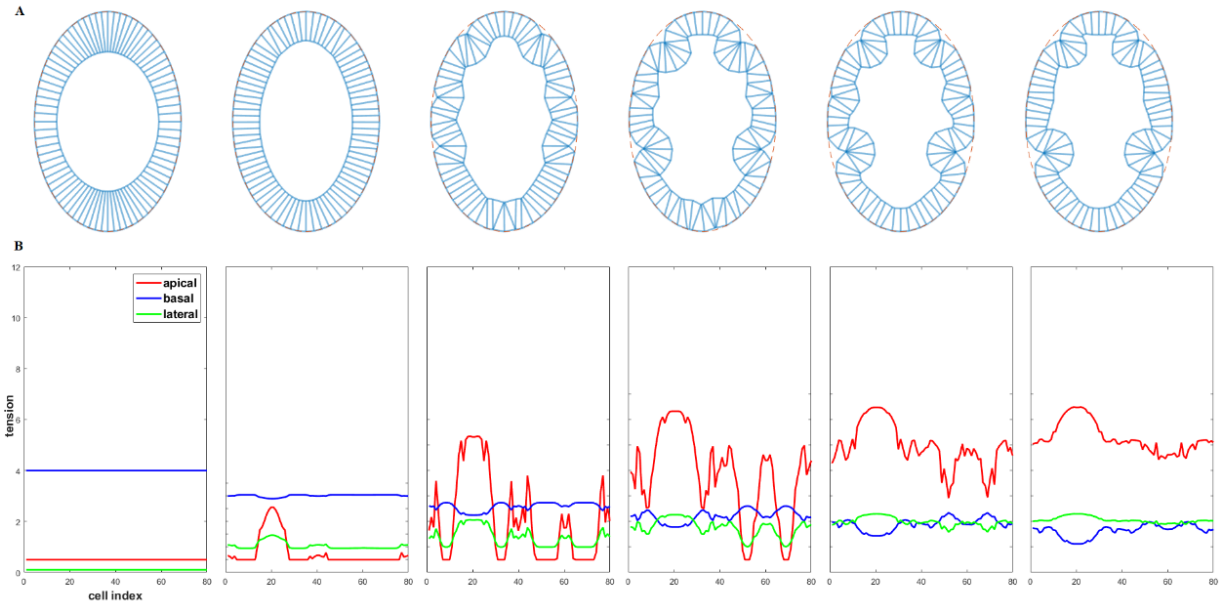

Figure 23 (A) elliptic compression (B) tension profiles correspond to shapes in (A). The time interval is 20% total simulation time. The red line is apical tension, the blue line is basal tension, and the green line is lateral tension.

Another set of simulations is to explore whether local ectopic compression would lead to ectopic invagination. To obtain an initial shape of local ectopic compression, we applied external apical forces peaking at the dorsal midline (Figure 24 Inset). We held the force for a certain amount of time while executing the energy minimization algorithm. The resulting shape (Figure 24) is used as the initial configuration for further simulations.

We retreated the external force at different time points to see if ectopic invagination could happen. It turns out that our model predicts the occurrence of ectopic invagination no matter when the external force is switched off. Holding the external force for a long time tends to stop mesoderm invagination (Figure 25).

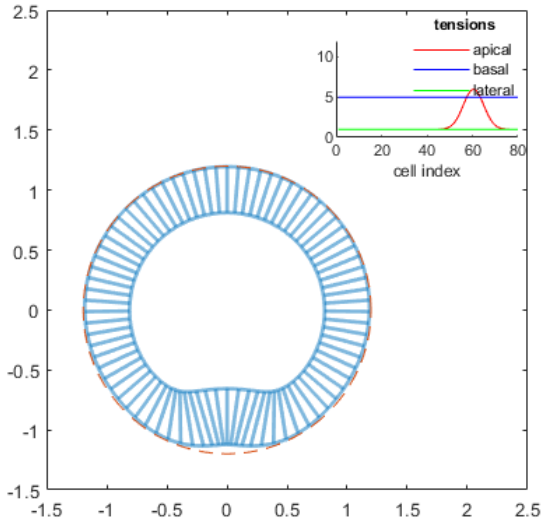

Figure 24 Initial local compression on the ectopic side with external tensions shown in the inset. 5000 iterations are used to obtain this shape.

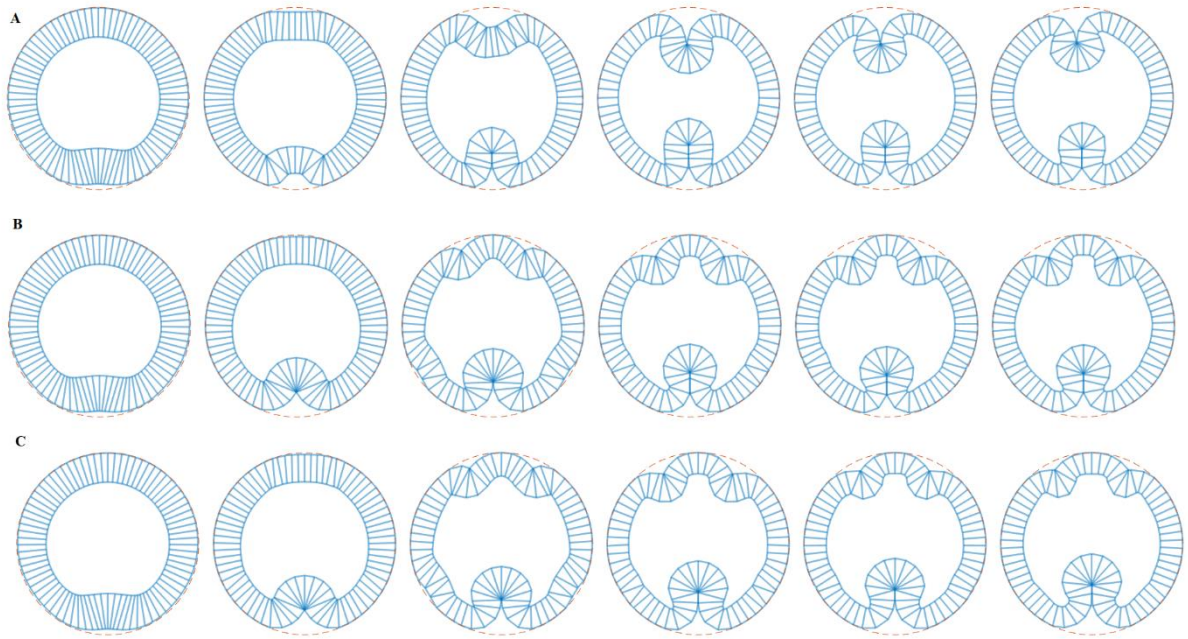

Figure 25 Time evolutions of tissue shapes in presence of external force. (A) Initial ectopic compression without external force. (B) hold external force for half of the total simulation time. (C) hold external force for the entire simulation.

The initial compression gradient on the dorsal side mechanically induces the expression of the *twist* gene, which sets up an ectopic force gradient. This force gradient amplifies the internalized curvature, promotes ectopic invagination with the help of increased lateral force. Relaxation of the ectopic invagination happens if the external force is turned off at the onset (Figure 25A), due to the competition between the mesoderm and ectoderm. In contrast, mesoderm

invagination is inhibited (Figure 25B and C) in the presence of a constant external force. Therefore, ectopic invagination does not relax. Abnormal apical constrictions still occur at both sides of the mesoderm boundary. As previously discussed, this results from the Hill function of mechanical feedback. The combined *twist* production term mediated by a Hill function (Eq 25) leads to a flat force distribution around the ventral midline, like a dome. Cells at the boundary of the "dome" feel higher force gradients and then deform the most. In the normal invagination process, the mechanical feedback term promotes those cells to contract first. That's why we observed mesoderm bending inward rather than apical constriction and radial shortening. While in the ectopic compression case, the mesoderm cells cannot bend inward without internalized curvature, therefore, the anomalous constriction happens instead.

In this chapter, we have discussed the modification of a vertex model to describe mesoderm invagination theoretically. We proposed a vertex model that uses an energy minimization algorithm to compute cell movements based on graded apical tension. We systematically studied the effects of different tensions and concluded that apical tension gradients are required for apical constriction. In addition, radial force and basal depletion are also necessary for apicobasal shortening. We put forth a set of regulation equations profiling active tension dynamics, in which we considered the mechanical effect on the production of the regulatory substance. We examined several configurations to investigate the influence of mechanical feedback. It turns out that our model can successfully invaginate under the control of regulation equations, although intermediate shapes do not strictly replicate experimental observation. The mechanical term behaves as expected, i.e. it will induce ectopic *twist* expression to flatten the force gradient, it will establish an ectopic *twist* gradient with the help of an external force. However, the tissue undergoes abnormal deformation due to mechanical feedback. This might be attributed to the simplicity of our model. A more complete regulation network must be considered.

Chapter 4: Conclusion

So far, we have introduced the total work of this master thesis project. Our goal is to provide a quantitative description of the mesoderm invagination during embryonic development of Drosophila from the underlying regulatory networks to tissue-wide shape changes.

Firstly, we reviewed previous studies on the biological side. We started with the genetic regulation pathways for epithelial morphogenesis of Drosophila embryos. The morphogen Spätzle sets up a gradient (Figure 2A) at the onset of gastrulation within a region defined by specific gene expressions (Moussian & Roth, 2005). That region is thought to be the presumptive mesoderm that will internalize to form a furrow during later stages. The Dorsal pathway (Figure 2B) is activated by the morphogen Spätzle in a graded manner, as well as its target gene *twist*. Expression of *twist* starts up the GPCR pathway leading to dynamic signaling transduction (Mason, Xie, Vasquez, Tworoger, & Martin, 2016) and pulsatile apical constriction (Martin, Kaschube, & Wieschaus, 2009). Differently, as another target gene of Dorsal, *snail* functions as a region-defining gene that uniformly distributes in the presumptive mesoderm and regulates signaling transduction downstream the GPCR pathway in parallel with *twist*. On the mechanical side, apical contractility is achieved by actomyosin networks and adherens junctions which account for cellular force generation and tissue-wide force propagation respectively. Sarcomere-like contractile units span radially over the apical surface of the cell, forming actomyosin networks. In the mesoderm, arrangements of actomyosin fibers can react to tissue-wide tension resulting in anisotropic contraction and leading to wedge-like cells rather than cone-like ones. Adherens junctions connect actin filaments of neighboring cells (Figure 4), thus transferring forces between cells (Chanet, et al., 2017). The stability of adherens junctions (Coravos & Martin, 2016) and the rearrangement of actomyosin networks (Hannezo & Heisenberg, 2019) suggest the presence of mechanical feedback, which is supposed to affect the conformations at the molecular level, as well as the production of regulatory substances (Farge, 2003).

In the second part, we introduced different types of theoretical models describing the mesoderm invagination. In the pioneering work of Odell et al. (Odell, Oster, Alberch, & Burnside, 1981), the individual cell consists of nodes and viscoelastic units. The presumptive mesoderm cells are excitable. The apical constriction is mediated by actively changing the rest length of the apical sides, such that mesoderm cells reach a stable state with contracted apical length. However, the contraction wave resulting from the excitable mechanism has not been observed yet, and intermediate shapes differ from experiments. The deformation gradient decomposition

method (Muñoz, Barrett, & Miodownik, 2007) uses experimental measurements as input. Cell movements are computed through the finite element method, in which the tissue is regarded as a continuum. The results emphasize the necessity of both apical constriction and apicobasal elongation/shortening. The vitelline membrane is necessary for a closed furrow formation. But the mechanisms leading to those active deformations are omitted. A model based on the collective instability hypothesis (Hočevar Brezavšček, Rauzi, Leptin, & Ziherl, 2012) reproduces mesoderm invagination as well, but with the least predefined cell attributes and active mechanisms. The invagination is the result of the collective response of the entire tissue. The assumption still needs to be verified experimentally. VFM (Conte, et al., 2010) provided a cellular force deducing method to reconstruct the active force distribution during mesoderm invagination. An apical force gradient is observed in mesoderm cells, which is consistent with the apical myosin intensity observed in vivo (Heer, et al., 2017). It also revealed that active tensions are dynamic during mesoderm invagination. The inverse algorithm is used to model the tissue with a given force profile (Conte, et al., 2012). The results suggest radial forces to be the determining factor for furrow depths. In contrast, a passive response of the tissue is demonstrated to be sufficient to drive ventral furrow formation (Polyakov, et al., 2014). Dynamically decreasing the basal stiffness can also lead to apicobasal shortening. This also confirmed the contribution of the vitelline membrane in terms of maintaining a circular tissue shape and forming a closed furrow. Nevertheless, active forces should also play a role in the morphogenic process as studied in (Conte, et al., 2012).

The thesis project aims to study the roles of active forces in mesoderm invagination and the connection between biological regulations and mechanical aspects mathematically. To this end, a 2D vertex model is the ideal theoretical basis. Because of the simple geometry of the tissue, the cell's mechanical properties can be easily attached to its sides and area, and the shape change is determined by nodal movements. In comparison to constant volume constraints used in the previously described models, we allow cells and the yolk to deform elastically by attributing an elastic energy term to them. Active forces are assigned to different sides of the cell. Passive mechanical responses result from the area elasticity and active deformations are originated from the corresponding line tension. The motion of every vertex is computed in parallel using an energy minimization algorithm. Based on this framework, we first explored the final shapes with various combinations for active forces in presence of an apical tension gradient. It turns out that the overall apical and basal tension levels maintain circular shapes of inner and outer contours. Furthermore, the lateral tension should be in a proper range such that it can provide enough radial shortening force and not lead to abnormal contractions. This range seems to be

small compared with basal tension levels, which is consistent with the relative magnitude observed in VFM (Conte, et al., 2010).

We systematically studied the influences of lateral and basal tensions with constant graded apical tensions. The results suggest that an apical tension gradient leads to apical constrictions and a corresponding inward curvature; basal expansion requires low basal tension levels; apicobasal shortening requires sufficient lateral tensions and is the dominant mechanism determining the furrow depth, which coincides with the previous study (Conte, et al., 2012). The final shapes with decreased basal tension and increased lateral tension correspond to stages observed in time series in vivo. The basal expansion may be originated from basal myosin depletion, which is thought to weaken the basal stiffness (Polyakov, et al., 2014). While in our model, the myosin depletion may directly reduce the active basal forces without changing cell mechanical properties.

After simulating with static line tensions, we then tried to apply forces with prescribed dynamics to the model. The results confirm that apical constriction can not promote mesoderm invagination on its own, apicobasal shortening and basal expansion are necessary for a successful furrow formation. These three mechanisms are corresponding to the apical tension gradient, lateral tension increment, and basal tension reduction respectively.

However, the time-dependences are predetermined. As for the mechanisms of tension dynamics, we set up reaction-diffusion equations trying to describe the observed dynamics. The entire regulatory network is complicated and thus difficult to put into a simple method. Therefore, the intermediate factors are omitted in our regulatory equations. We only considered the *twist* production utilizing the Gierer-Meinhardt equation for activator, the myosin concentration on each side is directly governed by the *twist*. Different self-regulatory terms are included to mediate basal myosin depletion and lateral increase. We added a Hill-type mechanosensing term to describe the *twist* induction by mechanical deformation. This term acts as positive feedback on apically contracted cells and negatively affects expanded cells. Our integrated model can replicate the mesoderm invagination, on the other hand, it can also reproduce graded apical myosin distribution, basal myosin depletion, and lateral myosin increase.

We also tested our model with different external constraints. An elliptic compression of the embryo leads to ectopic expression of *twist*, which smears out the *twist* gradient and thus also the apical tension gradient. This stops the mesoderm invagination from proceeding. Another constraint is the external force gradient. When an external force gradient is applied ectopically,

the tissue undergoes ectopic invagination due to the ectopic *twist* gradient induced mechanically. Switching off the external gradient may not fully relax the ectopic invagination since positive feedback has already set up the ectopic force gradient, but it relaxes once the mesoderm invagination has started. The persistence of the external ectopic force gradient stops the mesoderm invagination as well.

However, our integrated model also has some shortcomings. For example, the mechanical term makes a more rectangular apical tension profile which has a smaller gradient around the ventral midline and a larger gradient away from the ventral midline. This apical tension distribution leads to mesoderm bending rather than apical constriction and shortening in series, which differs from experimental observation. In addition, although the mechanical term could flatten the tension gradient and stop the invagination in the case of global compression, the tissue still has unexpected deformations due to the positive feedback, similar scenes also occur in the simulations with ectopic compression. A possible explanation would be that mechanical feedback is not the primary source of *twist* induction (Martin, 2020). In our model, the mechanical term and the Gaussian term are equally weighted, however, reducing the weight of the mechanical term fails to flatten the apical tension gradient in the simulations of elliptic compression (data not shown). Due to the simplicity of our regulatory network, details may be lost by neglecting the intermediate regulations. As a complement to the current model, one can explore other mechanisms that determine the contributions of mechanical feedback. Or one can come up with a new set of regulation equations that deal with the mechanical feedback more realistically.

In conclusion, we proposed a vertex model to study the mesoderm invagination and then integrated it with a regulatory network concerning mechanical feedback to simulate the active force dynamics. we considered the passive response and active line tensions simultaneously in our vertex model and can replicate the ventral furrow formation within a broad range of parameters. We concluded that the three mechanisms, apical constriction, basal expansion, and apicobasal shortening, are essential for mesoderm invagination. Losing any one of those results in unsuccessful invagination. The regulatory network is described by a series of reaction-diffusion equations, where *twist* is the only activator, to account for the tension dynamics. Mechanical feedback is a key feature of the regulation, it positively affects compressed cells and negatively affects stretched cells. The resulting tensions are still capable of mesoderm invagination to proceed. It also shows the failure in furrow formation in presence of ectopic *twist* production, which is consistent with the experiment. It predicts the ectopic invagination

with local ectopic compression due to the mechanical feedback, which requires a certain persistent time for the external compressive force. Our model exhibits abnormal deformations that deviate from experimental observations. Therefore, the actual mechanisms of mechanical feedback still need to be explored. The incompleteness of our regulatory network may lead to some important features letting missed. Thus, more detailed studies in the regulation are also needed.

References

Aegerter-Wilmsen, T., Heimlicher, M. B., Smith, A. C., de Reuille, P. B., Smith, R. S., Aegerter, C. M., & Basler, K. (2012). Integrating force-sensing and signaling pathways in a model for the regulation of wing imaginal disc size. *Development, 139*(17), 3221–3231. doi:https://doi.org/10.1242/dev.082800

Bardin, A. J., & Schweisguth, F. (2006). Bearded Family Members Inhibit Neuralized-Mediated Endocytosis and Signaling Activity of Delta in Drosophila. *Developmental Cell, 10*(2), 245-255. doi:https://doi.org/10.1016/j.devcel.2005.12.017

Barrett, K., Leptin, M., & Settleman, J. (1996). The Rho GTPase and a Putative RhoGEF Mediate a Signaling Pathway for the Cell Shape Changes in Drosophila Gastrulation. *Cell, 91*(7), 905-915. doi:https://doi.org/10.1016/S0092-8674(00)80482-1

Brodland, G. W., Conte, V., Cranston, P. G., Veldhuis, J., Narasimhan, S., Hutson, M. S., . . . Miodownik, M. (2010). Video force microscopy reveals the mechanics of ventral furrow invagination in Drosophila. *Proceedings of the National Academy of Sciences, 107*(51), 22111-22116. doi:10.1073/pnas.1006591107

Chanet, S., & Schweisguth, F. (2012). Regulation of epithelial polarity by the E3 ubiquitin ligase Neuralized and the Bearded inhibitors in Drosophila. *Nature Cell Biology, 14*(5), 467-476. doi:https://doi.org/10.1038/ncb2481

Chanet, S., Miller, C. J., Vaishnav, E. D., Ermentrout, B., Davidson, L. A., & Martin, A. C. (2017). Actomyosin meshwork mechanosensing enables tissue shape to orient cell force. *Nature Communications, 8*(1), 15014. doi:https://doi.org/10.1038/ncomms15014

Chopra, V. S., & Levine, M. (July 2009). Combinatorial patterning mechanisms in the Drosophila embryo. *Briefings in Functional Genomics, 8*(4), 243–249. doi:https://doi.org/10.1093/bfgp/elp026

Conte, V., Broadland, G. W., Cranston, P. G., Veldhuis, J., Narasimhan, S., Hutson, M. S., . . . Miodownik, M. (12 2010). Video force microscopy reveals the mechanics of ventral furrow invagination in Drosophila. *Proceedings of the National Academy of Sciences, 107*(51), 22111-22116. doi:10.1073/pnas.1006591107

Conte, V., Muñoz, J. J., & Miodownik, M. (2009). Robust mechanisms of ventral furrow invagination require the combination of cellular shape changes. *Physical biology, 6*(1), 016010. doi:https://doi.org/10.1088/1478-3975/6/1/016010

Conte, V., Ulrich, F., Baum, B., Muñoz, J., Veldhuis, J., Brodland, W., & Miodownik, M. (2012). A Biomechanical Analysis of Ventral Furrow Formation in the Drosophila Melanogaster Embryo. *PLOS ONE, 7*(4), e34473. doi:10.1371/journal.pone.0034473

Coravos, J. S., & Martin, A. C. (2016). Apical Sarcomere-like Actomyosin Contracts Nonmuscle Drosophila Epithelial Cells. *Developmental Cell, 39*(3), 346-358. doi:https://doi.org/10.1016/j.devcel.2016.09.023

Costa, M., Wilson, E. T., & Wiechaus, E. (25. March 1994). A putative cell signal encoded by the folded gastrulation gene coordinates cell shape changes during Drosophila gastrulation. *Cell, 76*(6), 1075-1089. doi:https://doi.org/10.1016/0092-8674(94)90384-0

Darsdo, D. (2000). Buckling Instabilities of One-Layered Growing Tissues. *Phys. Rev. Lett, 84*(18), 4244--4247. doi:10.1103/PhysRevLett.84.4244

Dawes-Hoang, R. E., Parmar, K. M., Christiansen, A. E., Phelps, C. B., Brand, A. H., & Wieschaus, E. F. (2005). folded gastrulation, cell shape change and the control of myosin localization. *Development, 132*(18), 4165–4178. doi:https://doi.org/10.1242/dev.01938

De Renzis, S., Yu, J., Zinzen, R., & Wieschaus, E. (2006). Dorsal-Ventral Pattern of Delta Trafficking Is Established by a Snail-Tom-Neuralized Pathway. *Developmental Cell, 10*(2), 257-264.

Farge, E. (2003). Mechanical Induction of Twist in the Drosophila Foregut/Stomodeal Primordium. *Current Biology, 13*(16), 1365-1377. doi:https://doi.org/10.1016/S0960-9822(03)00576-1.

Farhadifar, R., Röper, J.-C., Aigouy, B., Eaton, S., & Jülicher, F. (2007). The Influence of Cell Mechanics, Cell-Cell Interactions, and Proliferation on Epithelial Packing. *Current Biology, 17*(24), 2095-2104. doi:https://doi.org/10.1016/j.cub.2007.11.049

Fletcher, A. G., Osborne, J. M., Maini, P. K., & Gavaghan, D. J. (2013). Implementing vertex dynamics models of cell populations in biology within a consistent computational framework. *Progress in Biophysics and Molecular Biology, 113*(2), 299-326. doi:https://doi.org/10.1016/j.pbiomolbio.2013.09.003

Ganguly, A., Jin, J., & Ip, Y. T. (2005). Drosophila WntD is a target and an inhibitor of the Dorsal/Twist/Snail network in the gastrulating embryo. *Development, 132*(15), 3419-3429. doi:https://doi.org/10.1242/dev.01903

Gierer, A., & Meinhardt, H. (1972). A theory of biological pattern formation. *Kybernetik, 12*(1), 30-39. doi:10.1007/BF00289234

Goode, B. L., & Eck, M. J. (2007). Mechanism and Function of Formins in the Control of Actin Assembly. *Annual Review of Biochemistry, 76*, 593-627. doi:https://doi.org/10.1146/annurev.biochem.75.103004.142647

Gracia, M., Theis, S., Proag, A., Gay, G., Benassayag, C., & Suzanne, M. (2019). Mechanical impact of epithelial−mesenchymal transition on epithelial morphogenesis in Drosophila. *Nature Communications, 10*(1), 2951. doi:10.1038/s41467-019-10720-0

Grosshans, J., & Wieschaus, E. (26. May 2000). A Genetic Link between Morphogenesis and Cell Division during Formation of the Ventral Furrow in Drosophila. *Cell, 101*(5), 523-531. doi:https://doi.org/10.1016/S0092-8674(00)80862-4

Grosshans, J., Müller, H. J., & Wieschaus, E. (01. August 2003). Control of Cleavage Cycles in Drosophila Embryos by frühstart. *Developmental Cell, 5*(2), 285-294. doi:https://doi.org/10.1016/S1534-5807(03)00208-9

Grunewald, B., & Leptin, M. (1990). Cell shape changes during gastrulation in Drosophila. *Development, 110*(1), 73-84.

Hacker, U., & Perrimon, N. (1998). DRhoGEF2 encodes a member of the Dbl family of oncogenes and controls cell shape changes during gastrulation in Drosophila. *Genes&Development, 12*, 274-284. doi:10.1101/gad.12.2.274

Hannezo, E., & Heisenberg, C.-P. (2019). Mechanochemical Feedback Loops in Development and Disease. *Cell, 178*(1), 12-25. doi:https://doi.org/10.1016/j.cell.2019.05.052

Haskel-Ittah, M., Ben-Zvi, D., Branski-Arieli, M., Schejter, E. D., Shilo, B.-Z., & Barkai, N. (2012). Sef-Organized Shuttling: Generating Sharp Dorsoventral Polarity in the Early Drosophila Embryo. *Cell, 150*(5), 1016-1028. doi:10.1016/j.cell.2012.06.044

Heer, N. C., Miller, P. W., Chanet, S., Stoop, N., Dunkel, J., & Martin, A. C. (2017). Actomyosin-based tissue folding requires a multicellular myosin gradient. *Development, 144*(10), 1876-1886. doi:https://doi.org/10.1242/dev.146761

Hočevar Brezavšček, A., Rauzi, M., Leptin, M., & Ziherl, P. (2012). A Model of Epithelial Invagination Driven by Collective Mechanics of Identical Cells. *Biophysical Journal, 103*(5), 1069-1077. doi:https://doi.org/10.1016/j.bpj.2012.07.018

Ip, Y. T., Park, R. E., Kosman, D., Yazdanbakhsh, K., & Levine, M. (1992). dorsal-twist interactions establish snail expression in the presumptive mesoderm of the Drosophila embryo. *Genes & Dev, 6*, 1518-1530. doi:10.1101/gad.6.8.1518

Jha, A., van Zanten, T. S., Philippe, J.-M., Mayor, S., & Lecuit, T. (1. May 2018). Quantitative Control of GPCR Organization and Signaling by Endocytosis in Epithelial Morphogenesis. *Current Biology, 28*(10), 1570-1584. doi:https://doi.org/10.1016/j.cub.2018.03.068

Kölsch, V., Seher, T., Fernandez-Ballester, G. J., Serrano, L., & Leptin, M. (19. Jan 2007). Control of Drosophila Gastrulation by Apical Localization of Adherens Junctions and RhoGEF2. *Science, 315*(5810), 384-386. doi:10.1126/science.1134833

Krueger, D., Tardivo, P., Nguyen, C., & De Renzis, S. (2018). Downregulation of basal myosin-II is required for cell shape changes and tissue invagination. *The EMBO Journal, 37*, e100170. doi:https://doi.org/10.15252/embj.2018100170

Lecuit, T., & Yap, A. (2015). E-cadherin junctions as active mechanical integrators in tissue dynamics. *Nature Cell Biology, 17*, 533-539. doi:https://doi.org/10.1038/ncb3136

Leptin, M. (1991). twist and snail as positive and negative regulators during Drosophila mesoderm development. *Genes Dev, 5*, 1568-1576. doi:https://doi.org/10.1101/gad.5.9.1568

Lim, B., Levine, M., & Yamazaki, Y. (2017). Transcriptional Pre-patterning of Drosophila Gastrulation. *Current Biology, 27*(4), 610. doi:https://doi.org/10.1016/j.cub.2017.01.067

Manning, A. J., Peters, K. A., Peifer, M., & Rogers, S. L. (2013). Regulation of Epithelial Morphogenesis by the G Protein–Coupled Receptor Mist and Its Ligand Fog. *Science Signaling, 6*(301), ra98. doi:10.1126/scisignal.2004427

Martin, A. C. (March 2020). The Physical Mechanisms of Drosophila Gastrulation: Mesoderm and Endoderm Invagination. *GENETICS, 214*(3), 543-560. doi:https://doi.org/10.1534/genetics.119.301292

Martin, A. C., Gelbart, M., Fernandez-Gonzalez, R., Kaschube, M., & Wieschaus, E. F. (8. March 2010). Integration of contractile forces during tissue invagination. *Journal of Cell Biology, 188*(5), 735-749. doi:https://doi.org/10.1083/jcb.200910099

Martin, A. C., Kaschube, M., & Wieschaus, E. F. (2009). Pulsed contractions of an actin–myosin network drive apical constriction. *Nature, 457*(7228), 495-499. doi:https://doi.org/10.1038/nature07522

Mason, F. M., Tworoger, M., & Martin, A. C. (2013). Apical domain polarization localizes actin–myosin activity to drive ratchet-like apical constriction. *Nature Cell Biology, 15*, 926-936. doi:https://doi.org/10.1038/ncb2796

Mason, F. M., Xie, S., Vasquez, C. G., Tworoger, M., & Martin, A. C. (2016). RhoA GTPase inhibition organizes contraction during epithelial morphogenesis. *Journal of Cell Biology, 214*(5), 603-617. doi:https://doi.org/10.1083/jcb.201603077

Mata, J., Curado, S., Ephrussi, A., & Rorth, P. (26. May 2000). Tribbles Coordinates Mitosis and Morphogenesis in Drosophila by Regulating String/CDC25 Proteolysis. *Cell, 101*(5), 511-522. doi:https://doi.org/10.1016/S0092-8674(00)80861-2

Mathew, S. J., Rembold, M., & Leptin, M. (2011). Role for Traf4 in Polarizing Adherens Junctions as a Prerequisite for Efficient Cell Shape Changes. *Molecular and Cellular Biology, 31*(24), 4978-4993. doi:10.1128/MCB.05542-11

Morize, P., Christiansen, A. E., Costa, M., Parks, S., & Wieschaus, E. (1998). Hyperactivation of the folded gastrulation pathway induces specific cell shape changes. *Development, 125*(4), 589–597. doi:https://doi.org/10.1242/dev.125.4.589

Moussian, B., & Roth, S. (2005). Dorsoventral Axis Formation in the Drosophila Embryo—Shaping and Transducing a Morphogen Gradient. *Current Biology, 15*(21), R887-R899. doi:http://doi.org/10.1016/j.cub.2005.10.026

Muñoz, J. J., Barrett, K., & Miodownik, M. (2007). A deformation gradient decomposition method for the analysis of the mechanics of morphogenesis. *Journal of biomechanics, 40*(6), 1372-1380. doi:https://doi.org/10.1016/j.jbiomech.2006.05.006

Odell, G. M., Oster, G., Alberch, P., & Burnside, B. (1981). The mechanical basis of morphogenesis. I. Epithelial folding and invagination. *Developmental Biology, 85*(2), 446-462. doi:https://doi.org/10.1016/0012-1606(81)90276-1

Perez-Mockus, G., Mazouni, K., Roca, V., Corradi, G., Conte, V., & Schweisguth, F. (2017). Spatial regulation of contractility by Neuralized and Bearded during furrow invagination in Drosophila. *Nature Communications, 8*(1), 1594. doi:https://doi.org/10.1038/s41467-017-01482-8

Polyakov, O., He, B., Swan, M., Shaevitz, J. W., Kaschube, M., & Wieschaus, E. (2014). Passive mechanical forces control cell-shape change during Drosophila ventral furrow formation. *Biophysical journal, 107*(4), 998–1010. doi:https://doi.org/10.1016/j.bpj.2014.07.013

Prosser, C. L. (1974). Smooth Muscle. *Annual Review of Physiology, 36*, 503-535. doi:https://doi.org/10.1146/annurev.ph.36.030174.002443

Rahimi, N., Averbukh, I., Carmon, S., Schejter, E. D., Barkai, N., & Shilo, B.-Z. (1. November 2019). Dynamics of Spaetzle morphogen shuttling in the Drosophila embryo shapes gastrulation patterning. *Development, 146*(21), dev181487. doi:10.1242/dev.181487

Sawyer, J. K., Harris, N. J., Slep, K. C., Gaul, U., & Peifer, M. (2009). The Drosophila afadin homologue Canoe regulates linkage of the actin cytoskeleton to adherens junctions during apical constriction. *Journal of Cell Biology, 186*(1), 57-73. doi:https://doi.org/10.1083/jcb.200904001

Seher, T. C., & Leptin, M. (2000). Tribbles, a cell-cycle brake that coordinates proliferation and morphogenesis during Drosophila gastrulation. *Current Biology, 10*(11), 623-629. doi:https://doi.org/10.1016/S0960-9822(00)00502-9

Spahn, P., & Reuter, R. (2013). A Vertex Model of Drosophila Ventral Furrow Formation. *PLOS ONE, 8*(9), e75051. doi:https://doi.org/10.1371/journal.pone.0075051

Stephen Kerridge, A. M.-M. (2016). Modular activation of Rho1 by GPCR signalling imparts polarized myosin II activation during morphogenesis. *Nature Cell Biology, 18*(3), 261-270. doi:10.1038/ncb3302

Vasquez, C. G., & Martin, A. C. (2016). Force transmission in epithelial tissues. *Developmental Dynamics, 245*(3), 361-371. doi:https://doi.org/10.1002/dvdy.24384

Vasquez, C. G., Tworoger, M., & Martin, A. C. (2014). Dynamic myosin phosphorylation regulates contractile pulses and tissue integrity during epithelial morphogenesis. *Journal of Cell Biology, 206*(3), 435-450. doi:https://doi.org/10.1083/jcb.201402004

Weng, M., & Wieschaus, E. (2016). Myosin-dependent remodeling of adherens junctions protects junctions from Snail-dependent disassembly. *Journal of Cell Biology*, *212*(2), 219-229. doi:https://doi.org/10.1083/jcb.201508056

Xie, S., Mason, F. M., & Martin, A. C. (2016). Loss of Gα12/13 exacerbates apical area dependence of actomyosin contractility. *Molecular Biology of the Cell, 27*(22), 3526-3536. doi:https://doi.org/10.1091/mbc.E16-05-0305

Yap, A. S., Gomez, G. A., & Paron, R. G. (2015). Adherens Junctions Revisualized: Organizing Cadherins as Nanoassemblies. *Developmental Cell, 35*(1), 12-20. doi:https://doi.org/10.1016/j.devcel.2015.09.012